IN VIVO CONTACT MECHANICS OF THE DISTAL RADIOULNAR JOINT WITH AND WITHOUT SCAPHOLUNATE DISSOCIATION

By

Mathew Sunil Varre

Submitted to the graduate degree program in Mechanical Engineering and the Graduate Faculty of the University of Kansas in partial fulfillment of the requirements for the degree of Master of Science in Mechanical Engineering

_____

Chairperson: Dr. Kenneth J. Fischer

_____

Dr. Christopher Depcik

_____

Dr. Xinmai Yang

Date Defended:

The Thesis Committee for Mathew Sunil Varre certifies that this is the approved version of the following thesis:

IN VIVO CONTACT MECHANICS OF THE DISTAL RADIOULNAR JOINT WITH AND WITHOUT SCAPHOLUNATE DISSOCATION

_____

Chairperson: Dr. Kenenth J.Fischer

Date approved: 08/17/2011

Acknowledgements

First and foremost I would like to thank my advisor Dr. Kenneth J. Fischer for giving me an opportunity as his graduate student and providing all the necessary resources to bring this to pass. I thank him for all his input and assistance in ensuring that this project remained on track. I would like to thank my committee members Dr. Christopher Depcik and Dr. Xinmai Yang for all their invaluable support through the duration of my graduation studies. I also would like to thank my co-authors Dr. Bruce E. Toby, Dr. Terence McIff and Dr. Phil Lee for their support, valuable feedback and assistance in the project.

I extend my gratitude to all the Department of Mechanical Engineering faculty, staff and colleagues who gave in some part or another in this venture. I sincerely thank Allan Schmitt at the Hoglund Brain Imaging Center, University of Kansas Medical Center for his assistance with imaging.

I would like to thank my lab friends Joshua Johnson, Mahender Mandala, Michael Humphrey and Madhan S.Kallem for their assistance in the project and/or their valuable feedback in regard to various issues.

Last but not least, I would like to deeply thank my family and friends for their continued prayers and moral support without which my stay away from home alone would have been tough.

Abstract

The distal radioulnar joint (DRUJ) is a joint of the wrist which allows force transmission and forearm rotation in the upper limb while preserving the stability of the forearm independent of elbow and wrist flexion and extension. DRUJ is a commonly injured part of the body. Conditions affecting the joint could be positive ulnar variance or negative ulnar variance, the length of the ulna relative to radius. It is also adversely affected by nearby injuries such as distal radial fractures. In fact, a significant correlation was found between negative ulnar variance and scapholunate dissociation (SLD), a ligament injury of the wrist. This leads to the question of whether or not SLD causes changes in the radioulnar joint mechanics. Altered joint mechanics are associated with the onset of osteoarthritis (OA). An understanding of the of the normal and pathological wrist *in vivo* DRUJ contact mechanics should help physicians make better clinical recommendations and improve treatment for the primary injury. Proper treatment of the DRUJ could help prevent the onset of OA.

Image registration is used in our modeling to determine the kinematic transformations for carpal bones from the unloaded to the loaded configuration. A perturbation study was done to evaluate the effect of varying initial manual registrations and the relative image plane orientations on the final registration kinematics. The results of the study showed that Subject II (with different imaging plane orientations) was found to have greater translation errors compared to subject I (consistent imaging planes). This result emphasizes the need to be consistent with forearm position and/or image plane orientation to minimize the errors of translation and attitude vectors.

In a separate study, five additional subjects with unilateral SLD participated in another study in which magnetic resonance imaging (MRI) based contact modeling was used to analyze the contact mechanics parameters of the injured wrist compared to the normal wrist. The contact forces, peak contact pressures, average pressures and contact areas generally trended to be higher in injured wrists compared to the normal and surgically repaired wrists. Model contact areas were found to be consistent with the directly measured areas from the grasp MRI. A repeatability test was done on a single subject and the absolute differences between the contact parameters for both the trials were close. These findings suggest that SLD injury of the wrist may have an effect on the DRUJ mechanics.

Contents

List of Figures

Motivations and Research Objectives

The distal radioulnar joint (DRUJ) is one of the complex joint of the wrist. It allows the rotation of the forearm and transmits the force from the wrist to the forearm preserving the stability of the forearm. The DRUJ is affected by various nearby injuries such as distal radial fractures. Previous studies have shown that scapholunate dissociation (SLD) was found to have be correlated with the negative ulnar variance (relative length of ulna with the radius). SLD might alter the mechanics of the DRUJ which may lead to degeneration of the distal radioulnar articular cartilage.

Degeneration of the articular surfaces leading to joint dysfunction is known as arthritis and it is currently the most prevalent of the injuries of the joint diseases. Osteoarthritis (OA) is the most common form of arthritis and affects people all over the world and more often than not, leads to long term disability. OA is a degenerative joint disease, which involves progressive loss of articular cartilage, accompanied by attempted repair, remodeling and sclerosis of subchondral bone and osteophyte formation. Early signs include chronic joint pain, eventually resulting in loss of motion. This leads to the inability to perform day-to-day activities and loss in quality of life and has major impact on the economy [1]. OA of the hand and wrist is second only to the knee in terms of prevalence and prevention would go a long way in improving quality of life for many people.

The pathomechanics of OA is not known clearly. One of the factors resulting in joint degeneration leading to primary OA is believed to be excessive articular surface contact stresses. On the other hand, secondary OA occurs mainly as a result of injuries such as scapholunate dissociation that can alter both the kinematics and contact stresses. Magnetic resonance imaging

(MRI) based modeling can help assess in vivo contact mechanics. This method has been identified as a valuable tool for research [2]. It is a non-invasive means of evaluating contact characteristics from imaging data acquired during functional loading. Contact mechanics such as forces, contact areas and pressure distributions can be determined using this technique.

The availability of in vivo contact mechanics of DRUJ data may help determine the effect of scapholunate injury on the DRUJ mechanics. Contact patterns and intensities can be monitored using models over a period of time in order to observe change in kinematics or contact mechanics that might lead to joint degeneration. If an abnormality is observed, appropriate corrections could potentially be implemented to restore normal contact behavior and prevent occurrence of degenerative joint diseases.

In vivo contact mechanics data can provide a means to determine efficacy of surgical procedures used to repair joint injuries which might progressively lead to OA. Contact patterns can be compared before and after surgical reconstruction procedures to treat joint injuries. Longitudinal studies of injured human subjects, observed for a period of time to monitor for progressive, may identify key factors leading to OA.

Primary objective

The purpose of this study was evaluate to evaluate the contact mechanics of the DRUJ in wrist with scapholunate dissociation and in normal wrists based on MRI scans during functional loading. The hypothesis was that pressures and contact areas would be higher for injured wrists than for the normal and the surgically repaired wrists.

Secondary objective

The secondary objective of this study was to evaluate the effect of variations in initial manual registration of MR images on the final registration used for in vivo kinematic analysis of the DRUJ during grasp and also to evaluate how the registrations for two image sets from different imaging planes effects the accuracy of the final manual registration in this analysis. It was hypothesized that increased perturbations in initial conditions would result in increased errors in the final registration and that the bones imaged with different rotations (or imaging planes) would be registered with greater errors.

1 Background

1.1 Anatomy

The understanding of the anatomy is the basis for understanding the function of the human body. The human wrist is a complex and unusual series of multi-bone joints. Normal function depends on the integrated action of a number of tissue structures including the carpal and forearm bones, the intrinsic and extrinsic ligaments, tendons, and the components of the Triangular Fibro Cartilage Complex (TFCC). Because of the complex geometry, further research is needed to quantify the biomechanical measurements like joint contact areas, contact forces and peak contact stresses during functional loading. In order to understand this research, a brief description of forearm anatomy is given below. An understanding of the anatomy of the wrist will help distinguish between normal and abnormal conditions.

1.1.1 Forearm bones

Figure 1.1 Forearm in pronation (A) and supination (B) [public domain]

The forearm is the distal portion of the upper extremity from the elbow to the wrist (Fig 1.1). The forearm consists of two bones, the radius and ulna, and numerous muscles and ligaments. The radius and ulna bones contact each other at their proximal and distal ends. The annular ligament proximally at the elbow, interosseous membrane in the mid-forearm, and radioulnar

ligaments distally near the wrist stabilize the radius and ulna [3]. The motions of the forearm are pronation and supination and these play a vital role in hand and wrist function. At 90° elbow flexion, superior orientation of the dorsum of the hand is referred to as pronation while superior orientation of the palm is referred to as supination [4]. At the proximal end, the forearm bones articulate with the distal humerus of the upper arm, while at the distal end, they articulate with the proximal carpal bones of the wrist.

1.1.2 Bones of the wrist

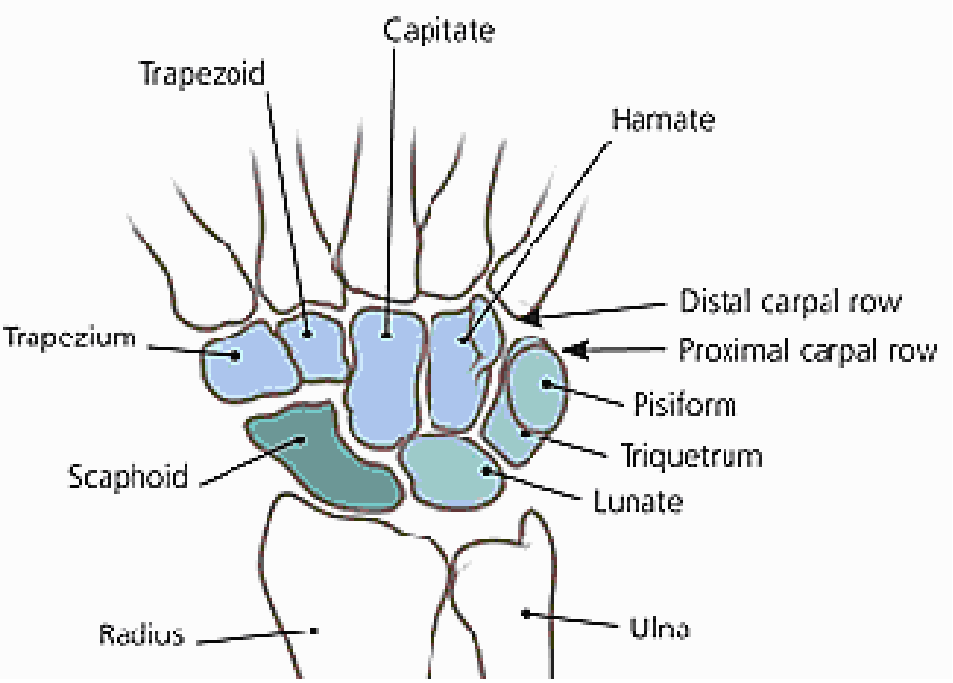

Figure 1.2 Wrist anatomy [public domain]

The wrist is a complex combination of bones and ligaments that connects the hand to the radius and ulna (Fig. 1.2). The wrist consists of the distal ends of radius and ulna, eight carpal bones, and the proximal bases of the metacarpals bones. The carpal bones are categorized as a proximal row and distal row on the basis of their anatomical location. The proximal row consists of scaphoid, lunate, triquetrum and pisiform, and the distal row consists of the trapezium,

trapezoid, capitate and hamate. The proximal carpal row bones can be described as an intercalated segment because no tendons insert upon them, and their motion is entirely dependent on the mechanical forces from their surrounding articulations [5, 6]. Only 50% of the motion in the wrist occurs at the radiocarpal joint. The remainder takes place in the mid carpal joint, the articulation between the two rows of carpal bones [5]. The distal row carpal bones are tightly bound to one another via stout intercarpal ligaments, and the motion between them can be considered negligible [5].

The distal radius contains concave fossa, one each for articulations with the scaphoid and lunate. When the wrist is loaded axially, the lunate and scaphoid rest in these fossa, pressing against the radius and each other. This is the radiocarpal joint. The ulnar head has two articular surfaces, the pole and the seat, which articulate with the triangular fibro cartilage complex (TFCC) and sigmoid notch of the radius respectively. The pole is U-shaped and is slightly curved, proximally curved towards the styloid and the seat is a conical surface that includes an articular cartilage. Approximately 75% of the ulna head is covered by articular cartilage [7-9]. A dorsomedial projection known as ulnar styloid can be seen on ulna to which a part of TFCC and ulnotriquetral ligament attach. Motion at the DRUJ occurs through the ulna, seated within the sigmoid notch, and the gliding undersurface of the fibro cartilaginous disk of the TFCC.

The DRUJ is the distal half of an articulation, and the proximal radioulnar joint is the proximal half of the articulation of forearm at the elbow. Thus DRUJ acts in concert with the proximal radioulnar joint as a bicondylar joint to control forearm rotation. The ulna represents the non-rotating, stable and load bearing part of the forearm around which the radius rotated in pronation and supination. The end of the radius together with the hand will rest against the stable ulnar head, which acts as key-stone to the wrist [10]. It is stabilized by the TFCC. This complex

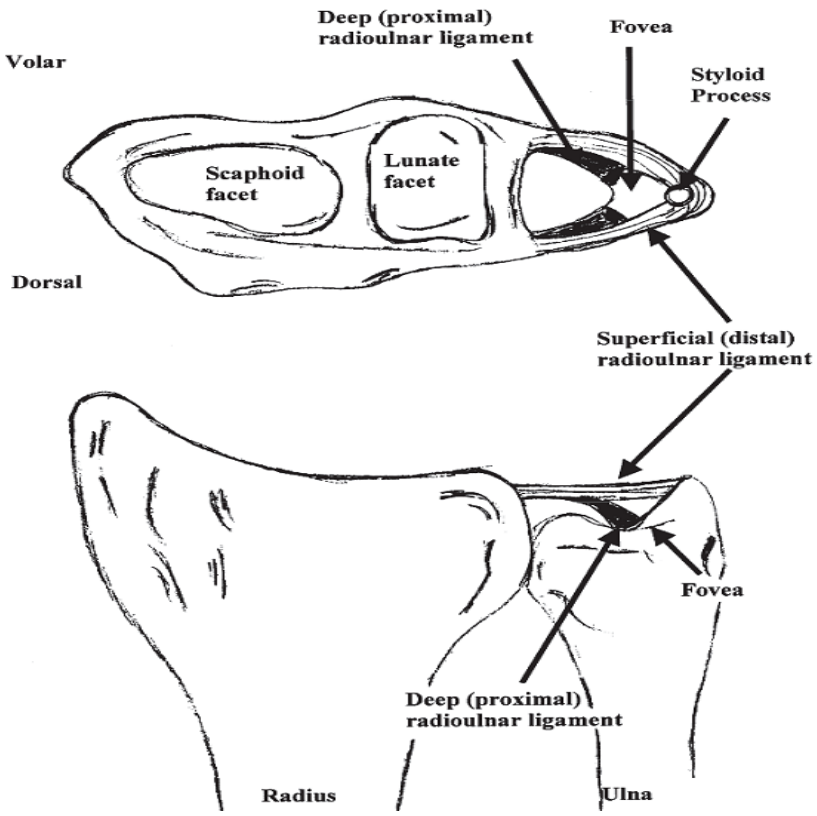

1.3 Distal radioulnar joint anatomy [11]

of fibro cartilage and ligaments support the joint through its arc of rotation, as well as provide a smooth surface for the ulnar side of the carpus. DRUJ is conferred stability through intrinsic and extrinsic mechanisms. Intrinsic mechanisms include the TFCC, the volar and dorsal radioulnar ligaments, the capsule, and the ulnar collateral ligament. Extrinsic stability is achieved through static and dynamic forces as the extensor carpi ulnaris (ECU) subsheath and the interosseous membrane (IOM). They are assisted by the pronator quadrates, which actively compresses the ulnar head into the sigmoid notch, and the extrinsic hand and wrist flexors and extensors, which dynamically compress the DRUJ. Radius carries about 82% of the load and ulna 18% of the load in the joint [10, 12, 13]. It is the distal radio ulnar joint that will be examined in this work [3, 9, 14].

1.2 Clinical issues

1.2.1 Injuries

With the growth and increase of popularity of the sports activities, athletes of all ages are pushing themselves to the limits to perform well. Injuries to the wrist are very common at all ages, ranging generally from the metaphyseal infractions of the childhood to the Colle's fractures at the older ages [11]. Distal radius fracture is one of the most frequent injuries in orthopedics [15, 16]. Distal radial injuries are mostly associated with the fractures at the distal radius. In younger or more physically active patients, malunion of the radius [17] may lead to DRUJ pain, limited motion, and decreased strength. Injuries to the DRUJ during trauma can occur as an isolated element or in combination with other injuries, mainly radius fractures. As there are both proximal and distal articulations between radius and ulna any injury to one of these could also affect the other. According to a report by Goldberg, the DRUJ is indirectly affected by almost 60% of the forearm injuries [18].

A thorough understanding of the osseous and ligamentous anatomy of the wrist is a fundamental requirement for any clinician attempting to understand and treat maladies of the carpus and the DRUJ. This information can be applied to find the normal joint mechanics and unravel the pathomechanics and improve the treatments procedures, making them anatomically and mechanically sound [14].

1.2.2 Dislocations of the DRUJ

Several authors have classified the disorders of the DRUJ based on various factors. Vesely's 'Classification of Affectation of the inferior radioulnar joint' included diseases which are congenital, developmental, disease metabolic, infectious degenerative and 'collagen diseases'.

Although, the classification of the disorders of DRUJ were helpful, they were not able to give needed guidance to the physicians on which treatment to use for an individual injury [10, 19, 20]. The most common fracture associated with DRUJ instability or dysfunction is the distal radial fracture. Malunited distal radial fractures may cause derangement of the DRUJ by creating instability, incongruity, or ulnocarpal impaction and even loss of motion.

Dislocation of the distal radioulnar joint can occur in an ulna dorsal or volar position relative to the radius. The deforming forces causing fracture instability are gravity, pronator quadrates, brachioradialis and thumb abductor and extensors. Ulnar dorsal dislocation is caused by hyper pronation associated with a fall. Other mechanism that might cause this condition may be direct isolated force to the ulna and radius, respectively. This dislocation may be due to disruption of the dorsal ligaments with partial or complete injury to the TFCC. Volar dislocations of the distal radioulnar joint are associated with forced associated supination stress of the forearm or a direct blow to the ulnar aspect of the forearm [21, 22].

Instability of the DRUJ has been generally defined on the basis of the direction the ulnar head moves in relation to the distal radius. Bowers defined stability as a repeatable path of the articular contact on the normal arch in the restricted motion of the joint and instability as 'the abnormal path of the articular contact occurring during or at the end of the arc of motion attempted [20]. Instabilities of the DRUJ and TFCC are together classified as stable, partially unstable (subluxation) or unstable (dislocation) [11, 16, 22-24].

1.2.3 Fractures

Fractures of the DRUJ involve either the distal ulna or the articulating sigmoid notch of the radius. Distal ulna fractures may occur as isolated injuries or in combination with the distal

radial fractures. Isolated fractures of the ulnar styloid process can occur at the tip or at the base. The injury may be caused by forced deviation, high rotatory stresses or even extreme wrist dorsiflexion [23]. It can also occur as impaction or avulsion type injuries. Fractures to the distal ulnar head usually result from significant trauma and are commonly accompanied with radial fractures. This injury can involve distal ulnar head and styloid process or just the distal ulnar head. Distal radial fractures frequently include fractures through the sigmoid notch usually secondary to an injury caused by fall on a dorsiflexed wrist [21, 24]. In a 'die-punch' fracture the lunate loads the lunate fossa with the fracture line progressing into the distal radioulnar joint [22, 25, 26].

Dislocations of the DRUJ are more often accompanied by distal radial fractures. Colles' fractures and Smith's distal radial fractures often are associated with dislocations of the DRUJ [22]. Galeazzi's fractures, Essex-Lopresti Lesions and bone-bone forearm fractures can also result in the dislocations of the distal radioulnar joint [27]. In addition, injuries to the carpus, as well as forearm and elbow or even growth plate injuries can be associated with distal radioulnar joint injuries [28].

1.2.4 Ulnar Variance

Ulnar variance refers to the relative lengths of the ulna and radius. The relative length of the ulna compared to the radius is an important element in wrist pathology. A short ulna is defined as negative ulnar variance and a long ulna results in positive ulnar variance. Negative ulnar variance has been associated with Keinbock's disease, avascular necrosis of the scaphoid and scapholunate dissociations. Positive ulnar variance is harmful to the ulna compartment of the wrist as it causes degeneration and perforation of the TFCC and cartilaginous wear of the carpal bones. Ulnar variance is also a determinant of the morphology of the sigmoid notch of the radius.

The length of the ulna compared to the radius differs between individuals and also may change during one's lifetime [29]. Ulnar or radial lengthening and shortening procedures for Keinbock's disease or settled 'Colles' fracture have made the need of determining the ulnar variance more important.

Palmer et al. developed a simple, accurate and reproducible method of measuring ulnar variance from standard posteroanterior radiographs of the wrist [30]. The distance between contiguous articular surfaces of the distal radio carpal and ulnocarpal joints (and, thus ulnar variance) changes with wrist and forearm position [31]. Supination increases the measurement of negative ulnar variance and pronation decreases the measurement of the negative ulnar variance. [32].

Czitrom et al. studied the effect of ulnar variance on the carpal stability of the wrist for scapholunate and lunotriquetral dissociations. Since the proximal articular surfaces of the lunate articulate with both radius and ulna, there is a possibility that perilunate injuries might correlate with the ulnar variance. A significant correlation has been found between negative ulnar variance and scapholunate dissociation [33].

1.2.5 Ulnar Impaction Syndrome

The ulnar impaction syndrome, also termed the ulnocarpal abutment syndrome, can be defined as a degenerative condition of the ulnar side of the wrist related to excessive load bearing across the ulnar carpus, triangular fibro cartilage complex, and the ulnar head. These compressive forces result in ulnar wrist symptoms such as pain and limited motion secondary to a variety of pathological changes that are most commonly a result of positive ulnar variance [34]. Ulnar impaction syndrome can be a result of day-to-day activities such as lifting loads and

contact sports, that result in excessive intermittent loading on the ulnar carpus. Dynamic increases in ulnar variance may accompany forceful grip and pronation making the diagnosis difficult. Excessive compressive load may be transmitted across the ulnocarpal joint even in the ulnar neutral or negative wrist because the thickness of the articular disc of TFCC is inversely proportional to the amount of ulnar variance and variance may increase with functional activity [35]. Therefore, it can occur in wrists with either neutral or negative variance. Treatment is directed at reducing the load on the ulnar head by shortening the distal ulna in one of the several treatment methods such as wafer, Sauve-Kapandji, Darrach procedures. Ulnar shortening by recession is a preferred treatment for relative stability of the ulnar ligamentous complex [36]. Ulnar impaction resulting from the malunion of the distal radius can be corrected by radial osteotomy [37]. Darrach procedure is effective as a salvage procedure. Hence, careful preoperative evaluation and planning are important for successful treatment of ulnar impaction syndrome [38, 39].

1.2.6 Ulnar Impingement Syndrome

Ulnar impingement syndrome is caused by a shortened ulna impinging on the distal radius and causing painful, disabling arthrosis [40]. Growth arrest of the bone after fracture with epiphyseal damage may also be a possibility for the shortened ulna. Symptoms are weak grip, wrist pain and clicking wrist during pronation and supination. The most common cause for the shortened ulna is the excision of the ulna. Excision of ulna is mainly recommended in the treatment of traumatic dysfunction of the distal radioulnar joint and sometimes also for subluxation of the ulnar head, rheumatoid arthritis and the correction of Madelung's deformity [41]. The excision mainly aims at the reduction of the pain and increase in the range of movement after the fracture of the radius and ulna. However, this procedure reduces the grip

strength due to the impingement of the ulna. Radioulnar convergence is observed in most of the cases in addition to narrow wrist. This condition can be avoided by treating the distal radioulnar joint by reconstruction rather than shortening the ulna in younger patients. In elderly patients or in case of rheumatoid arthritis, excisional arthroplasty may be adequate. Repairs of the shortened ulna using extensor carpi ulnaris as a tendonesis are more helpful in restoring the stability and also to deal with the radioulnar convergence. Treatment of the unequal growth can be done by either radial shortening or ulnar lengthening with reconstruction of the distal radioulnar joint. [41].

The most common complaint after distal radial fractures is ulnar sided wrist pain. Fractures and dislocations of the distal radioulnar joint are often seen as a secondary problem to the direct radius fracture [22]. Because DRUJ issues are often not diagnosed, in the long run distal radius fractures cause ulnar wrist pain secondary to DRUJ incongruity. Therefore in the evaluation of the injuries in the forearm, DRUJ must be properly assessed clinically and radiographically. This assessment would help determine if DRUJ instability exists and allow various treatment procedures in order to stabilize the joint.

1.2.7 Scapholunate Dissociation

The most common carpal instability is scapholunate dissociation with dorsal intercalated segment instability [42]. DRUJ instability is not only caused by a malunion but also due to ligament injuries. An understanding of the normal anatomy and recognition of abnormal pattern in the radiographs will help in proper diagnosis of these uncommon injuries. Often, instability is not diagnosed because the ligamentous injuries are not visible in a radiograph [43]. Scapholunate dissociation is the most frequent serious ligamentous injury of the wrist and when it is not treated properly, it generally leads to disabling wrist pain, reduced wrist mobility and chronic

degenerative arthritis. This injury frequently occurs in persons who participate in activities requiring repetitive wrist rotation, especially gymnastics, tennis, golf and basketball. Typically, the injury is sustained when the patient falls on the out stretched hand with wrist in extension, the forearm in pronation and the impact of the fall occurring on the thumb. Acute injuries need to be treated by operative repair of the ruptured ligaments with temporary stabilization of the scaphoid [44]. Long term pain reduction and maintaining wrist stability could be achieved with ligament reconstruction, limited wrist arthrodesis, interosseous reconstruction or triscaphe fusion [45]. Magnetic resonance imaging (MRI) is the only imaging technique that can directly depict abnormalities of the ligaments. Patients with chronic scapholunate dissociation and extended degenerative abnormalities of radius-scaphoid or capitate-lunate joints require extensive wrist reconstruction although it reduces the mobility of the wrist [42, 45].

1.2.8 Osteoarthritis

Osteoarthritis (OA) is the most common joint disease and is among the most frequent and symptomatic health problems for middle aged and older people [1]. OA is characterized by pain in the joint and dysfunction caused by joint degeneration, a process that includes progressive loss of cartilage [1]. In advanced stages of OA, joint contractures, muscle atrophy and limb deformity can be observed. The pathomechanics of OA, which result in joint degeneration, are not known. OA also develops as a result of injuries or a variety of hereditary, inflammatory, or developmental, metabolic, and neurologic disorders, a group of conditions referred to as secondary OA (usually due to injury). Primary OA occurs in people older than 40 years. Secondary OA, caused by joint injury may occur in younger adults. The incidence of OA rapidly increases with each passing decade after an age of 40 years in all joints [1, 46].

The presence of intra-articular fracture of the distal radius can lead to the development of premature arthritis of the radiocarpal, ulnocarpal and distal radioulnar joints [47]. Previous studies have shown that residual articular incongruity of 1-2mm during fracture healing is associated with radiographic evidence of arthrosis [47]. In contrast, two studies have concluded that symptomatic arthritis is rare after intra-articular distal radius fractures despite radiographic evidence of arthrosis [48]. This may be due to the fact that wrist is not a weight bearing joint [1, 48].

1.2.9 TFCC Tears

Triangular Fibro Cartilage Complex (TFCC) is the primary stabilizer of the DRUJ and a part of it, named triangular fibro cartilage (TFC) or articular disk, is a triangular structure interposed between the distal ulna and the ulnar carpus. The TFC rises from the distal radius and inserts into distal ulna and into the lunate, triquetrum, hamate and base of the fifth metacarpal [14]. The TFCC acts as a stabilizer for the distal radioulnar joint and the ulnar carpus along with being as a load-bearing cushion for the transmission of axial loads between the ulnar carpus and the forearm unit [49, 50]. With the TFCC intact, the radius bears approximately 82% and ulna 18% of axial loading. When the TFCC is excised, the load borne by the radius increases up to 100% [12]. In addition, TFCC contributes to the stability of the ulnocarpus [23].

Through their studies, Palmer and Werner showed that almost 18% of the compressive loads across the wrist are transmitted to the ulnar head through the TFCC in neutral variance position. Previous studies have shown the association of increased positive ulnar variance with the incidence of TFCC injuries [23]. This can be attributed to the increase in compressive loads on the TFCC due to increase in positive ulnar variance [12, 13]. Palmer classified the TFCC disorders as Traumatic (Class 1) or degenerative (Class 2) which in turn are further sub classified

according to the location of the disruption. Persistent pain after radius fracture is common and can result in chronic instability [36]. Ulnar sided wrist pain may be caused due to tears of the TFCC. Pain due to tears of TFCC may be attributed to either DRUJ instability or altered fluid dynamics of the radiocarpal and distal radio ulnar joints or perhaps from mechanical internal derangement of the joint.

1.3 Biomechanics of the DRUJ

The primary function of the DRUJ is forearm rotation. The distal radius rotates about ulna up to 150 degrees (60-80 pronation and 60-85 of supination) [7, 12]. Studies have shown that ulna has subtle but significant translation with rotation. Short et al. found that 80% of the joint reactive force across the wrist is borne by the radiocarpal joint. Furthermore, a radiocarpal joint reaction force is distributed between the scaphoid and lunate facets at approximately 60% and 40%, respectively [13]. Shabaan and his co-workers investigated the force transmission through DRUJ in cadaveric specimens in various forearm positions. They found that force transmitted across the DRUJ was higher in supination than pronation [51].

Bowers theoretically predicted that pressure will increase in the dorsal portion and decrease in the volar portion of the sigmoid notch in pronation and that the opposite occurs in supination [20]. A similar study was done by Ishii et al. using a fujifilm pressure sensors and they observed similar patterns [52] confirming Bower's prediction. Crisco et al was successful in measuring *in vivo* 3-D carpal kinematics using non invasive CT imaging [53]. Neu et al. used cadaveric specimens in order to find carpal kinematics in a 3-D wrist study [52, 54]. The surgical procedures altering the natural length of the radioulnar length, significantly affect the contact pressures at the DRUJ and load transmitted by the forearm. This *in vitro* study could not estimate the *in vivo* contact areas as the sensor can alter the congruity of the joint [52].

Treatment of the distal radial fractures using procedures such as Darrach resection, Sauve-Kapandji procedure and implant arthroplasty not only compromise the function of the joint but also altered the anatomy at the distal radius leading to the dysfunctioning of the DRUJ [4]. Radial shortening of more than 10 mm made the fracture instable [55, 56]. In a cadaveric study, the load acting on the radius relative to the ulna was measured in different positions of the wrist and forearm for cadaveric specimens with osteotomized bones [57]. It was found that there was less load acting on the radius longitudinally in wrist flexion, ulnar deviation and full forearm pronation.

Werner et al. investigated the effect of the ulnar lengthening and shortening on the force transmitted through the radioulnar carpal joint [58]. A change in the length of the ulna may result in a large change in the forces borne by it. Ulnar shortening of 2.5mm reduces the load acting on the ulna from 18.4 % to 4.3 % of the total force. Lengthening of ulna by 2.5mm increases the force borne by the ulna to 42% of the total forearm force. Removal of ulnar head completely shifts the load to the distal radius. Radial deviation of the wrist decreased the load borne by the ulna, and ulnar deviation decreased the load as well [10, 58]. These changes lead to unpyhsiological loading patterns and may increase the risk of secondary degenerative arthosis at the point of contact where the stress is concentrated [26, 58].

Viegas et al. evaluated the effect of radio ulnar stability on the radio carpal joint using a Fuji film [59]. It was found that, in supination there was a decrease in lunate contact area for all stages of radioulnar stability. In a joint with ulnar styloid fracture, scaphoid and lunate pressure areas were found to be more palmar (volar) than in a normal joint. Effect of change in length of ulna was investigated in a study on cadaveric specimens using pressure sensitive films [58, 60]. Ulnar lengthening by 2.5mm increased the peak Ulno lunate pressure by a factor of two. Ulna

shortening decreased this by a factor of one-quarter [58]. It has also been found that the interosseous membrane can transfer forces between the radius and the ulna [59].

Understanding the normal kinematics helps in effectively diagnosing wrist pathology and planning surgical treatment of traumatic and or degenerative changes of the wrist joint. Motion of a joint can be measured precisely by identifying the center of rotation. However, DRUJ does not have a single center of rotation as the radius has both translation and rotation relative to the ulna [61]. King et al. determined the centers of rotation for the DRUJ using a contour matching technique based on computed tomography (CT) images [61].

Most of the studies previously done were *in vitro*. Various techniques such as anatomic dissection, soft tissue sectioning and electromagnetic motion tracking have been used in the past to determine DRUJ kinematics [62]. According to af Ekenstam et al. [57] and Hagert [8] the dorsal radio ulnar ligament becomes taut during supination and restrains displacement of radius dorsally. Schuind et al. (1995) found that the dorsal radioulnar ligament increased in tension during pronation and volar radioulnar length increased during supination. Mirachi et al. (2008) analyzed radio ulnar joint and found the kinematics of the DRUJ are complex, involving both static and dynamic stabilizers [6, 8, 63].

Although testing on the cadaveric specimens has laid the foundation for understanding DRUJ kinematics, they have been limited because of *in vitro* biomechanical experimentation and anatomical studies with no attempt to simulate *in vivo* muscle loading. Errors due to soft tissues' compensation and disruption in the joint also affected the kinematics in such studies [17, 64]. Previous *in vitro* studies were not able to show the out of plane motion of the carpal bones. *In vivo* non-invasive measurement of kinematics avoids usage of marker techniques and allows

incorporation of muscular forces. It also helps evaluate the long term effect of the surgical intervention and procedures and healing. *In vivo* studies of DRUJ kinematics have been limited to 2-D centrode analysis. The 3-D kinematics of the DRUJ have not been evaluated yet. Powerful imaging techniques such as CT and MRI have allowed for the non-invasive 3-D motion analysis of DRUJ. This advancement in imaging techniques will help understand how the kinematics were altered due to injury compared to the normal joint. Researchers have measured non-invasive *in vivo* 3-D kinematics of the wrist joint using 3D images. Moore and his research team found that DRUJ kinematics were not altered in malunited wrists [17, 65].

Crisco et al was successful in measuring in vivo 3-D carpal kinematics using non-invasive CT imaging. Neu et al. [66] used cadaveric specimens to find carpal kinematics in a 3-D wrist study. Many researchers used electromagnetic measuring systems as they do not involve radiation and require only small sensors fixed to a bone. However, most of these studies were related to forearm position and not the wrist in specific [52, 53, 67, 68]. Leonard et al. [69] developed a simple non-invasive method of measuring and modeling the wrist joint motion that could be used to improve the kinematic performance of the wrist arthroplasty designs. They used an electromagnetic system to record the wrist motion in all three dimensions. An iterative computer model was developed using a two-axis hinge, the output of which gives the offset of the two axes of motion, which gives the radioulnar deviation in the wrist. The three dimensional motion plots generated from this model could be used clinically to follow disease progression and the recovery following surgery. The mathematical analysis of the recorded motion patterns helped improve wrist arthroplasty design.

Helical axes of motion parameters were used to describe the motion of the radius with respect to ulna in various forearm positions [17]. Sommer et al. [70] described a general

technique for fitting spatial kinematic model to an in-vivo anatomical joint under typical physiological loading conditions. Patterson et al. used an optical motion analysis system to find the kinematics of carpal bones [71]. These results were similar to a cadaveric study where carpal kinematics were measured using CT based non-invasive position registration methods [72].

Usage of registration methods to determine motion transformations non-invasively has been common in the past decade with advancement in technology and the availability of common software. Surface registration and volume based registration techniques were used to generate kinematics by extracting contours from images [73].

In CT scan based methodologies to study 3-D motion of bones *in vivo* joint surface, shape or moment of inertia were used for determining the kinematics [17, 62]. *In-vivo* CT scan images with surface registration using Analyze software (Analyze Direct, Overland Park, KS, USA) was used to quantify radioulnar motion in wrist of patients who had distal radial fractures [17]. Neu et al. [66] found that kinematic accuracy depends on the registration method and bone shape and size. They studied the kinematic accuracy of three surface registration techniques in a 3-D wrist bone study. They also reported that marker less bone registration techniques could provide accurate measurements for 3-D non-invasive in vivo kinematics of any skeletal joints. Fischer et al. [74] used a registration block technique for determining the experimental kinematics of an in vitro study. Drawback of surface registration is that registration accuracy is limited to the accuracy of the segmentation of the images. Goto et al. [73] non-invasively analyzed 3-D motions of the wrist in vivo using MR Images in which they compared surface registration with volume registration. Volume based registration was found to be more accurate than surface-based registration for both translation and rotational component. However, errors introduced due to segmentation and image acquisition could not be avoided and effect the final results.

1.4 Modeling

Modeling is an investigative technique that incorporates mathematical, computer, or physical depictions of a system to conduct research on that system. The advent of computers and evolution of processing power has vastly improved the study of human motion in part due to the relative ease of computer model construction and reduction in processing time to generate a solution. A model is very useful in the exploration of biomechanical parameters affecting the human body. To understand the distal radioulnar joint, it is beneficial to have the knowledge of the methods commonly used in biomechanical engineering. The constraints and limitations of experimental methods have led to greater usage of computational methods in biomechanical studies. Computational methods are not affected by physical limitations and risks, repeatability and environmental conditions. Moreover, they are not restricted by subject variability; however, it may not be possible to generalize subject-specific models [75-78].

The procedure for most of the modeling techniques intrinsically has the basic steps of creation of models, deriving equations of motion for the models, programming a numerical solution, determining the boundary conditions and finally the results obtained from the computation, interpretation and comparison with experimental data .

The two main methods of model simulation used in biomechanical studies are finite element method (FEM), and Rigid Body Spring Modeling (RBSM). The RBSM has become quite popular recently, due to its simplicity and computational efficiency in contact analysis. n recent times, a third method has been developed. This method uses a surface based contact modeling approach, which generally provides for more accurate interface and more flexible contact rules, while maintaining computational efficiency.

Despite the sophistication and appeal of modeling over experimental methods, computational modeling does have some limitations, which arise from factors such as numerical imperfections in the solution process, difficulty of acquiring accurate physiological material properties, approximation of complex human anatomy and in vivo boundary conditions.

1.4.1 Imaging Techniques

The history of imaging the hand and wrist is the history of the radiology itself. The very first x-ray was of the hand [79]. The first clinical application of the X-rays in the United States revealed a Colle's fracture. Radiography is the use of X-rays to view non-uniformly composed materials by utilizing the properties of the ray. Other imaging techniques used to evaluate injury are conventional radiography, tomography, computed tomography (CT), arthrography, angiography, digital radiography, scintigraphy and magnetic resonance imaging (MRI) [80]. Medical imaging has undergone a rapid development with a strong emphasis being placed on the use of imaging technology to render surgical and therapeutic procedures less invasive and to improve the accuracy with which a given procedure can be performed compared with conventional methods [81]. In imaged guided therapy (surgery, radiotherapy or radiological intervention), pre operative medical data, usually 3-D CT or MR images, are used to diagnose, plan, simulate, guide, or otherwise assist a surgeon or a robot in performing a surgical or therapeutic procedure [79, 82].

All diagnostic imaging of the hand and wrist generally begins with radiographs or plain films. Plain radiographs with physical examination are usually sufficient for the work up of a painful hand or wrist [81]. It produces 2-D representations of a 3-D anatomical data on a photographic film or digital receiver. The standard views used for most anatomical areas are frontal and lateral projections. Care has to be taken in aspects of positioning, radiographic

exposure for proper diagnosis. The radiograph is the most commonly used imaging tool for hand and imaging the wrist even though several new and technically advanced imaging techniques such as CT and MR imaging have been developed. However, when radiographs fail to elucidate the cause of the symptoms, CT and MRI studies may be required [82].

Tomography is the method of using radiography to produce images of a single plane within the body. The simplest form of tomography is linear tomography. For a hand and wrist, thin slices are required because of the small size and complex geometry of the bones. Linear tomography is limited by the inability to blur the linear shadows created during the imaging process due to tube motion [82]. Therefore, the structures to be imaged need to be placed perpendicular to the direction of motion whenever possible. Poly directional-tomography is advancement over linear tomography in order to overcome the problems of linear streaking by using a complex pathway for tube motion relative to the film [82]. This technique is efficient in demonstration of subtle fractures and arthodeses producing extremely clear details of even small structures of the hand and wrist. Computed tomography is advancement in the tomography methodology. It uses axial motion of the x-ray tube to create the planar image as opposed to coronal or saggital direction of motion in conventional tomography [82].

Imaging complicated anatomies is extremely difficult even with newest technologies. With advancement in technology available in high resolution MRI, the interpretation between normal and abnormal conditions has become less difficult. MRI is commonly used to the evaluate the joints for internal derangements [83]. MRI of the wrist has been used in the evaluation of a wide spectrum of diseases. Its multiplanar and exquisite soft tissue contrast capabilities allow for depiction of subtle osseous and soft tissue pathology. Although the anatomy is complex, indications from MR imaging would be helpful to understand anatomy and pathology [82, 84].

1.4.2 Model development from images

One of the main highlights of the computational modeling is the non-invasive simulation of various loading conditions, from which a medical perspective provides insight about the anatomy and physiological conditions of the human body. These models help understand the mechanisms of various conditions such as acute injuries, repetitive and excessive stresses and degenerative diseases like Osteoarthritis. Accurate models provide clinicians and biomedical engineers an investigative tool that increases the basic knowledge in order to better the existing treatment procedures for detection, prevention and cure with an improved or new approach.

Accurate representation of the anatomy and material properties of the human tissues is very important in understanding the underlying mechanisms leading to joint disorders of the body. Developing computational models of the human joints with accuracy is a complex process, which begins with acquiring images of the anatomy to be analyzed. The most common methods acquire images of bone, soft tissue, or a combination of both, which are then used to create 2-D or 3-D models. X-ray images are sometimes used to create highly accurate 2-D models. Imaging techniques such as CT and MR imaging are used to generate 3D models. CT scan images are generally used to generate highly accurate models of bone, but the soft tissue near the bones cannot be imaged accurately. MRI has lower contrast and signal to noise ratio (SNR), and is used to model both bone and soft tissues such as cartilage. Quality of the image largely depends on the application.

The process of generating models from images involves three basic stages of segmentation, compilation and surface mapping. The first step of segmentation involves extracting geometry of the anatomy of interest from individual images in the image set. For images acquired using CT scan, the boundaries are often segmented automatically using

threshold methods. MRI contours are usually segmented manually. The second step involves combining all the individual contours in each image set into a point cloud. Finally, surface mapping is used to develop a surface description based on the 3-D point cloud.

1.4.3 Finite Element Modeling

Current technological advancements demand the need of accurate analyses of very large and complex structures. Irregularities in geometry, varying material properties and multiple loading conditions make accurate and efficient solutions difficult to achieve. Due to the increasing power of computers, more accurate and complex analyses can be performed using the finite element method.

Most of the complex systems can be reduced to a set of small elements (finite). These finite elements can be analyzed in combination to obtain a solution for the system as a whole. This process of reduction into small elements is called discretization. This process provides us with polynomial approximations on these elements and numerical approximation can be obtained. Finite element method is a numerical technique which involves analysis of a system that is an assembly of a finite number of discrete elements interconnected at nodes. After the domain is described as mesh of finite elements, approximation of the response of the system based on the behavior of the individual elements would be easier. Some of the advantages of FEM include accuracy of the results, convergence of approximations, and ability to determine stresses and strains inside a tissue [85-90].

Finite element modeling consists of the following steps. The first step is the idealization of the structural system that involves selection of type and size of the finite elements to generate a numerical mesh of the system. One of 1, 2 or 3 dimensional elements defined by n^{th} order

polynomials can be selected depending on the computational time and accuracy of solution required. Geometric and elastic properties of each individual element in the system are defined. Boundary conditions are described including definition of the loading conditions. Finally, operations are performed to generate matrix equations by use of principle of minimum energy. These matrix equations are solved to obtain displacements, strains and stresses throughout the model. Building highly accurate finite element meshes can also be time consuming even with semi-automated meshing. Automatic meshing generally yields an inferior mesh in some locations.

FEM generates highly accurate solutions, not for just the surface, but throughout the entire volume of the analysis. It is capable of simulating both static and dynamic loading conditions. However, the solution process often involves intense computation based on the number of equations and the order of differential equations being solved. Often, this is further complicated by the non-linearity associated with surface contact and/or material properties which is often the case when dealing with biological systems. Regardless of the number of elements, FEM provides an approximate solution only. The higher the number of elements and polynomial order of the differential equations, the higher the accuracy. However, this in turn increases the computational time. Therefore, it comes down to a balance between computational time and accuracy of the solutions.

Anderson et al. developed a plane-strain finite element contact model of the radiocarpal joint to investigate the relationship between intra articular fracture of the distal radius, subsequent imprecise reduction of the articular in congruency and final onset of the osteoarthritis [91]. For this analysis, the FEM of the radiocarpal joint was generated using scaled anatomical drawings of the distal radius, scaphoid and lunate bones. A mesh consisting of 1291 quadrilateral elements

was created with material properties based on values previously reported in the literature. Nonlinear spring elements were used to model ligamentous attachments between the three bodies with stiffness properties based on those reported by Hori et al. No prior assumptions were made regarding the details of the load transfer across joint surfaces in this contact coupled model. Contact was modeled in this model using slide line elements allowing finite deformations and finite sliding between bodies with Coulomb friction as the criteria. A frictional coefficient of 0.01 was designated for all articular surfaces. Results showed that the distribution of the load between the radius and ulna was similar to previous experimental data [7, 12]. The plot of axial strains supports the role of articular cartilage as a load distributing mechanism across the articular surfaces and the strains were on the order of 20 to 25%. Stress distributions obtained with finite element model were consistent with previously published data for other articular joints.

Ulrich et al. used 2D FEM for load transfer analysis of the distal radius trabecular network from *in vivo* high resolution CT images to determine the effect of tissue loads leading to fracture in those regions [92]. Tissue strain energy density distribution was used to characterize load transfer through the trabecular network. High resolution images of the left distal radius and adjacent carpal bones were taken using low-dose peripheral quantitative computed tomography (pQCT) with a slice thickness of 0.165mm. These scan images were used to generate 3D FEM models using a voxel conversion technique, and layers of cartilage of thickness 3 mm were added artificially. The entire FE mesh consisted of 1,679,025 elements and all material properties were obtained from the literature. Four different loading regimes were applied to the carpal bones (with the proximal radius fully constrained) representing impact forces on the hand either in near neutral position or ulnar/radial deviation. Two FEM problems were solved, each

containing one of the carpal bones loaded with a unit force and the other unloaded. Post processing involved superimposing and scaling of displacement fields and calculating strain energy density and von Misses stress. It was demonstrated that with this technique the distribution of tissue loading in bones in vivo could be estimated. Results indicated that the radius had high strain energy values for all loading cases. This suggests that common regions of fracture are likely due to high tissue strain energy density values in the trabecular network.

Ledoux et al. studied the mechanisms of modifications to the mechanical behavior of the carpus after a scaphoid fracture led to the onset of arthritis of the wrist [93]. The bone geometry was traced based on an anterior- posterior x-ray of a healthy wrist. Trapezium and Trapezoid were modeled as a single block of bone. A 2D FE mesh of different skeletal elements was generated using an automatic mesh generator defining 1053 nodes. Ligaments and cartilage were assigned with non-linear type properties such that cartilage can undergo only compression and ligaments only tension. A simulated load of 100N was applied to the metacarpals at the level of radius and ulna. The model predicted that peak pressures exist at the non-union and lunate-capitate and scapho-capitate articulations and that the amount of load carried through the radiolunate fossa increased dramatically during the scaphoid fracture. The study also showed that there was a significant increase in pressure at the articular surface due to the scaphoid fracture.

Carrigan et al. developed a 3D FE model to analyze the load transmission pathways in the constrained carpus (neutral posture) during static compressive loading. The bone geometry (carpal and metacarpal) was extracted from *in vivo* CT scan FE meshes were generated for individual bones from these scan images and compiled in ANSYS to assemble carpal geometry. This model was used to analyze various parameters under static compressive loading of the wrist in the neutral posture. The articulating cartilage layers in the solid geometry were modeled as 15-

node triangular prism. Ligaments were modeled using non linear, tension-only spring elements and material properties of all solid elements were defined to be linearly elastic based on prior FE studies. An axial load of 15N was applied to the capitate for all cases and a series of parametric sensitivity cases were analyzed to determine the impact of various factors like changes in cartilage modulus on contact pressures and cartilage stresses. The model results show that cartilage material properties and unconstrained carpal rotation have substantial effect on the articular contact patterns and pressures [94].

1.4.4 Rigid Body-Spring Modeling

The rigid body theory is a fundamental and well-established theory of physics. Rigid body spring models are based on the assumption that force applied to the bodies produces negligible deformation. In applying this method to skeletal structures, it is presumed that the deformation of the bones can be neglected when compared to the deformation of the cartilage layers at the contact surfaces. The cartilage is modeled as a set of compressive springs on the surface of the bone, which is considered rigid. Ligaments are modeled as tensile springs that hold the bones together. This method provides a computationally efficient means of determining joint forces and ligament tension without the need for a more complex FE analysis [95].

Garcia-Elias et al. developed a 2D model of the transverse carpal arch using RBSM. The contours of the joints were generated from the MR images. Compressive springs were distributed over the surface of the modeled cartilage. The ligaments of the carpal arch were modeled using tensile elastic springs. This model was then used under simulated dorsopalmar compression to calculate the relative motion between the carpal bones, the distribution of compressive forces in the intercarpal joint, and the tensions in the ligaments. Results showed that the palmar hamate-capitate ligament plays a significant role in stability of the carpal arch [96].

Horii et al. created a 2D RBSM of the wrist to evaluate the force and pressure transmission between the carpal bones. In this model, carpal bones were modeled as rigid bodies and connected to each other with elastic springs. X-rays were used to obtain bone geometry. Reaction forces between carpal bones were modeled using a system of linear elastic springs; cartilage was modeled as linearly compressive springs and ligaments as tensile linear springs. The spring constraints were determined based on material and structural properties of ligaments and cartilage taken from literature. Axial loads were applied along the metacarpals to simulate grasp of 10 N with the wrist in neutral position. It was found that the force transmission ratio was 55% through the radioschaphiod joint and 35% through the radiolunate joint. The remaining load was observed in the triangular fibrocartilage. The scaphoid was found to have the largest percentage of load amongst the intercarpal bones [97].

In a nearly identical study, Schuind et al, created a 2D RBSM of the wrist. Schuind found similar percentages of force transmission in the three contacts (radioscaphoid 50%, radioluante 30% and TFCC 15%). It was determined that the peak pressure occurred at the proximal pole of the scaphoid. Results showed no significance of age on wrist force distribution and that wrist morphology had little influence on the magnitude and pattern of load distribution.

1.4.5 Multi Body Contact Modeling

Surface contact modeling is a numerical procedure used for complex structural analysis of rigid or deformable interacting bodies, based on a contact rule. There are a number of programs existing presently with which a broad range of systems can be modeled. The most attractive feature of contact modeling is the ability to generate solutions more quickly than the continuum based FE methods, using highly efficient algorithms. Also, contact modeling does not make priori assumptions about details of load transfer across the joint surface. The nature and

distribution of these loads are determined from the computations involved in the contact model. Therefore, multi body contact modeling has been used to model biomechanical systems as well, including diarthrodial joint modeling. The main drawback of the multi-body contact modeling is its inability to analyze the stresses and strains throughout the solid, that may be obtained using FEM.

Kwak et al. developed a very general 3D multi-body model specifically designed for the analysis of arthrodial joints, under quasi-static conditions. These models included articular contact for the between arbitrarily shapes surfaces, and wrapping of soft tissues around bone and the articular surface and tendon forces as pulleys. The material bodies, bones in this case, were modeled with six degrees of freedom (three rotations and three translations), while the particles are typically imbedded in the soft tissue structures such as tendons and ligaments, which wrap around the articular surfaces with three translational degrees of freedom. The imbedded particles redirect the ligaments and tendons force while transmitting the resultant contact force onto body around which they are wrapped. Ligaments were modeled as links connecting the insertion points on the two distinct bodies along a series of line segments with the forces acting along the direction of the line. Muscle force was simulated as a special case of the ligament link in the model as a constant force applied along a line segment which inserts on the separate bodies. A tendon-pulley link was used to simulate the tendon spanning multiple diarthrodial joints. Contact between the articular surfaces of the bones was simulated using a surface contact link where surface deformation and resulting contact stresses within a contact region were approximated using a proximity function which is an overlap of rigid surfaces. These models were implemented using input files which contained geometric entities, link parameters and initial body poses with several different force displacement ligament models and cartilage deformation

implemented as non-linear/linear models. Cartilage and bone surfaces were represented using piecewise triangular facets to be efficient in calculation of surface-surface contact and particle-to-surface contact. Results obtained were found to be within the prescribed convergence criteria and were further validated using patellofemoral joint models constructed from six cadaver knees and compared to the experimental data [98].

Pillai et al. [99] conducted a study to evaluate *in vivo* wrist joint mechanics using MRI based contact modeling. The geometry for the contact models was obtained from MRI scans of the non-dominant wrist of four human subjects using a 1.5 Tesla clinical MRI scanner with a flex wrist coil. Scans were performed during light active grasp of a 30mm cylinder and during relaxed state with the forearm in neutral position. The position of the wrist was not strictly controlled during grasp scan. Manual segmentation of the radius and carpal bones (lunate and scaphoid) including articular surfaces was performed on the relaxed image sets to obtain contour data which were then used to generate 3D surface models. The three bones, excluding articular surfaces, were isolated from the grasp and relaxed image sets in order to determine transformation from the unloaded to loaded configuration. Using the radius as a fixed reference, a series of surface registrations were performed in order to obtain kinematics (rotation and translation vectors) for both lunate and scaphoid. The kinematic parameters along with geometric entities were given as input in joint_model program, a multi body contact software based on Kwak et al. [2] for contact analysis. The contact rule was defined as a cartilage thickness of 1 mm and material properties were acquired from literature. *In vivo* contact pressures, areas and forces were analyzed for each articulation and found to be in reasonable agreement with previous studies. This study showed MRI based contact modeling to be a valuable technique in evaluating *in vivo* joint contact mechanics [100].

Thoomukuntla et al. [101] performed a study to validate the MRI based modeling approach developed by Pillai et al. Model geometry was acquired from MR scans of the wrist of three cadaver forearm specimens. Volar dissection of the wrist was performed to insert pressure (static film and electronic) sensors for direct measurements while three flexor tendons (FDS, FDP and FPL) were isolated to simulate light grasp when loaded. To maintain consistent neutral forearm position, the forearms were attached to a base plate. Direct measurements were taken by inserting pressure sensors into dissected joint space and loading the tendons in light grasp. Similarly, MR scans of the wrist were taken in both unloaded and loaded configurations, which were used to generate 3D models. Radius was used as the fixed reference. The kinematic transformations of the carpal bones from the unloaded to the loaded states were obtained using a series of image registrations. These along with the model geometry were loaded into the contact modeling software Joint_Model [2] for contact analysis. Results compared between pressure sensors and MRI based models were reasonable. Also, contact areas were directly measured from loaded MR scans and these were found to match closely with model results [102].

Waller [103] further validated the technique proposed by Pillai et al. and Thoomukuntla et al. Five cadaver specimens were used and similar procedures followed based on Thoomukuntla. Five tendons (two extensors and three flexors) were isolated for joint loading in this study. After kinematics and contact analyses, contact area obtained from models were similar to direct contact area measurements from grasp MR scans, contact forces similar to Tekscan measurements and peak pressures similar to Pressurex measurements. These results further validated the MRI based modeling technique to be feasible for joint contact analysis, and this approach was used as the basis for the work done in this thesis applied to the DRUJ by Johnson [104].

Johnson [104] validated the MRI based radiocarpal models generated from a 3T clinical MR scanner for future *in vivo* joint contact analyses. Three cadaveric forearm specimens were used in this study. The bones and tendons of concern were isolated and the radiocarpal capsule was also dissected to insert the film. Two extensors and 3 flexors were also isolated during dissection. During simulated light grasp, pressure was measured using Pressurex film and Tekscan sensor, and was compared to the contact mechanics data obtained from contact modeling. MRI scans were taken in a 3T clinical scanner for both loaded and unloaded configurations. Models of radius, scaphoid and lunate were created from the MRI images. The kinematics were obtained by a series of image registrations. These kinematics were applied in the modeling software Joint_Model to obtain contact parameters such as contact force, contact pressure and contact area, which were compared with experimental data. Results obtained were comparable to those obtained in the previous radiocarpal contact validation studies made by Waller [103] and Thoomukuntla et al. [102].

Most of the previous *in vitro* studies discussed were developed as a means of evaluating *in vivo* joint mechanics to determine the effects of injury and the efficacy of surgical repair. The overall goal was to provide insight into pathomechanics leading to joint degeneration.

The present study adopts the same modeling approach used by Johnson [104] for his thesis, to evaluate the *in vivo* contact mechanics of the DRUJ. Although, the DRUJ is less congruous when compared to the radiocarpal joint, MRI based contact modeling is applicable to evaluating the *in vivo* contact mechanics of the distal radioulnar joint with and without a scapholunate injury, as well as investigating the efficacy of the surgical repair for restoring the normal mechanics of the DRUJ.

2. Effect of Different Imaging Plane Orientations and Varying Initial Manual Registration on Final Image Registration for Radioulnar Joint

2.1. Introduction

The wrist is a complex joint composed of radiocarpal, the intercarpal, the meniscal carpal and the radioulnar joint [13]. Distal radioulnar joint (DRUJ), is a complex joint comprised of two forearm bones (radius and ulna) and various soft tissues such as the triangular fibro cartilage complex (TFCC), dorsal and volar radioulnar ligaments and the oblique fibers of the distal interosseous membrane [12, 64, 105, 106]. The complex articulation of this joint depends on both soft tissues and bony stability, which allow for forearm rotation, but preserves the DRUJ stability independent from elbow and wrist flexion and extension [30, 31, 107, 108]. Understanding the normal kinematics helps in effectively diagnosing wrist pathology and surgical treatment of traumatic and or degenerative changes of the wrist joint [10]. Clear understanding of DRUJ injury instability and effectiveness of reconstructive procedures is also quite important, because forearm rotation is indispensible in activities of daily living [61, 108].

A number of biomechanical studies have been performed to define the kinematics of the normal wrist and changes in the kinematics of joints in various degenerative states [109]. The investigators mostly relied on x-ray films and cadaveric specimens to observe the relative motions in the wrist. Various techniques such as soft tissue sectioning with electromagnetic motion tracking have been used in the past to determine DRUJ kinematics [62]. DRUJ does not have a single center of rotation as radius has both translation and rotation relative to ulna [61]. Mirachi et al. [63] analyzed the radioulnar joint and found the kinematics of the DRUJ to be complex, involving both static and dynamic stabilizers. Neu et al [66] used cadaveric specimens to find carpal kinematics in a 3-D wrist study. Patterson et al [110] used an optical motion analysis system to find the kinematics of carpal bones. These results were similar to work done

by Kauffman et al [72] who measured carpal kinematics using CT based non-invasive position registration methods in cadavers. Fischer et al [74] used registration block technique for determining the experimental kinematics in an *in vitro* study.

The analysis of cadaveric kinematics has been widely used to investigate the effects of pathologies, trauma and reconstructive procedures on joint motion. *In vitro* studies can be advantageous in studying the effects of the injury and repair on acute joint stability [53]. Although *in vitro* studies have laid the foundation for understanding DRUJ kinematics, most *in vitro* biomechanical experimentation and anatomical studies have studied passive motions, with no attempt to simulate *in vivo* muscle loading. Errors due to soft tissue attenuation and disruption in the joint could have altered the kinematics in such studies introducing potential errors [17, 64]. *In vivo* non-invasive measurement of kinematics avoids usage of marker techniques and allows incorporation of muscular forces. It also helps evaluate the long term effect of the surgical intervention and procedures and healing [65]. *In vivo* studies of DRUJ kinematics were limited to 2-D analysis in the initial stages [47] and the 3-D kinematics of the DRUJ have only recently been evaluated [111]. With the advent of powerful imaging techniques such as CT and MRI, methodologies have been developed for the non invasive 3-D motion analysis of DRUJ based on these imaging techniques [53, 65, 67, 112]. This advancement in imaging techniques helped to understand how the kinematics were altered due to injury compared to the normal joint. Researchers have measured non-invasive *in vivo* 3-D kinematics of the wrist joint using 3D images [108, 113]. Moore and his research team found that DRUJ kinematics was not altered in wrists injured with distal radial fractures [17, 65].

Using image registration methods to determine motion transformations from non-invasive image data has become common in the past decade with advancement in technology and

availability of software. Surface registration and volume based registration techniques were used to generate kinematics by aligning images. The methodology used to determine kinematics can affect the final kinematics of the bones in any joint, including normal and injured wrists [66, 73]. Based on CT scans, some investigators have studied the 3-D motion of bones *in vivo* by registering bone surface, volume or geometric moment of inertia. For example *in vivo* CT scan-based surface registration ANALYZE software was used to quantify radioulnar motion in wrist of patients who had distal radial fractures [17]. However, Neu et al [66] found that kinematic accuracy depends on the registration method and bone shape and size. They studied the kinematic accuracy of three surface registration techniques in a 3-D wrist bone study and reported that markerless bone registration techniques can provide accurate measurements for 3-D non-invasive *in vivo* kinematics of any skeletal joints. The drawback of surface registration is that registration accuracy is limited to the accuracy of the segmentation of the images. Goto et al [73] analyzed non-invasively 3-D motions of the wrist *in vivo* using MR images in which they compared surface registration with volume registration. Volume based registration was found to be more accurate than surface based registration for both translations and rotations [62, 73]. However, errors introduced due to segmentation and image acquisition could not be avoided and can affect the final registration results. Nobody has studied the combined effect of the initial registration conditions and differences in the bone imaging plane on the final registration in a kinematic analysis of a joint.

The purpose of this study was to evaluate the effect of variations in initial manual registration on the final registration for *in vivo* kinematic analysis of the distal radioulnar joint during grasp. The other aim was to evaluate how the registrations for two image sets from different imaging planes effects the accuracy of the final manual registration in this analysis. It

was hypothesized that increased perturbations in initial conditions would result in increased errors in the final registration and that the bones imaged with different rotations (or imaging planes) would be registered with greater errors.

2.2. Methods

Two healthy human subjects participated in this study. The human subject protocol and consent forms were approved by the Human Subjects Committee of the University of Kansas Medical Center. The MRI was done at Hoglund Brain Imaging Center located at the University of Kansas Medical Center with a 3-Tesla MRI Scanner (Allegra, Magnetom Vision Plus, Siemens, Malvern, PA). A Constructive Interference Steady State (CISS) pulse sequence and a custom made double loop surface coil around the wrist joint were used. Both subjects had two scans, one with the hand relaxed and a second taken during light grasp. The relaxed scan was taken with a slice thickness of 0.5 mm thickness and a pixel size of 0.15 mm. The light grasp scan was done with a slice thickness of 1.0 mm and a pixel size of 0.3 mm. The subjects were asked to maintain constant grip pressure during the scan using a visual feedback system. For Subject 1 (S1), both scans were performed with the forearm in supination position. For Subject 2 (S2), the relaxed scan was performed with the forearm in supination position and the light grasp scan was performed with forearm in neutral rotation.

Images obtained were segmented to isolate radius and ulna individually on a black background for individual bone image registration. Image registration was performed using ANALYZE 5.0 (AnalyzeDirect, KS, USA) with a combination of manual and automatic 3D voxel registrations to obtain a best fit. The registration gives a transformation for the alignment of the bones in unloaded state to the loaded state. The basic assumption for the kinematic analysis was negligible deformation of the bone during light grasp. For this study, the radius was

selected as the reference (fixed) bone. The loaded radius was registered to the unloaded radius, to determine the kinematic transformation from the loaded to the unloaded image coordinate system (to align image sets). This transformation was then used to transform the loaded ulna to the unloaded image coordinate system. Lastly, the unloaded ulna was registered to match the transformed loaded ulna, which provided the desired kinematic transformation.

For each instance of registration, manual registration of the bones was performed carefully to obtain a standard manual registration for each bone. The Standard Best Match (SBM) was obtained in two steps: 1) by performing automatic registrations for 25 consecutive iterations beginning from the standard manual registration and 2) manually selecting the best match SBM from the 25 auto registration iterations. To assess the effect of manual registration errors, perturbations were introduced to the standard manual registration. Translation perturbations of one to three pixels were applied to the standard manual registration, automatic registrations were again performed, and a perturbation best match (PBM) was manually selected from the 25 consecutive auto registrations. This procedure was repeated for translation perturbations in each coordinate direction. Similarly rotation perturbations of 1°, 2°, or 3° about the X, Y or Z axis were applied to the standard manual registration to obtain additional perturbed initial conditions and the PBM for each rotation perturbation was selected as in translation perturbations. The PBM transformation for each perturbation was compared to standard best match using RMS errors of translation and rotation vectors.

2.3. Results

Table 2.1 and Table 2.2 show the RMS errors averaged for radius and ulna along perturbation level and direction. It can be seen that the translation and rotation perturbation vector magnitudes were generally of very small magnitude.

2.1Magnitude of the translation and rotation errors averaged over perturbation level about X, Y, Z directions for each of translation (T pixels) and rotation (R degrees) perturbations for radius and ulna

		Radius						Ulna					
Subject	Perturbation	Translation vector			Rotation Vector			Translation vector			Rotation Vector		
		X	Y	Z	X	Y	Z	X	Y	Z	X	Y	Z
I	T(pixels)	0	0.0117	0.0212	0	0.0002	0.0004	0.0246	0.0246	0.0468	0.0003	0.0003	0.0006
	R(degrees)	0.0473	0.0627	0.0290	0.0005	0.0007	0.0004	0.0460	0.2390	0.0271	0.0005	0.0025	0.0005
II	T(pixels)	0	0.1426	0.1556	0	0.0026	0.0023	0	0.0710	0.2040	1.2800	0.0493	1.0500
	R(degrees)	0.0414	0.1448	0.0492	0.0016	0.0014	0.0003	0	0.0006	0.0028	0.0137	0.0073	0.0124

2.2 Magnitude of the translation and rotation errors averaged over each direction along 1, 2, 3 pixels/degrees for each of translation (T pixels) and rotation (R degrees) perturbations for radius and ulna

		Radius						Ulna					
Subject	Perturbation	Translation vector			Rotation Vector			Translation vector			Rotation Vector		
		1	2	3	1	2	3	1	2	3	1	2	3
I	T(pixels)	0	0.0095	0	0.0003	0.0002	0	0.0395	0.0395	0.0164	0.0005	0.0005	0.0002
	R(degrees)	0.0383	0.0579	0.0427	0.0004	0.0006	0.0005	0.1253	0.0791	0.1079	0.0015	0.0008	0.0011
II	T(pixels)	0.1426	0.1018	0.0538	0.0017	0.0026	0.0007	0.0705	0.0473	0.1572	0.8717	1.0559	0.8940
	R(degrees)	0.0254	0.0962	0.1138	0.0003	0.0019	0.0012	0.0009	0.0007	0.0019	0.0113	0.0133	0.0088

The translation perturbations of the radius and ulna resulted in RMS errors of translation and rotation vectors (averaged over perturbation level and direction) that were higher for S2 than S1 (Fig 2.1). Rotation perturbations for the radius also resulted in higher errors for S2 than for S1. Finally rotation perturbations of ulna yielded higher errors for S2 rotation, but slight lower errors for S2 translations, compared to S1.

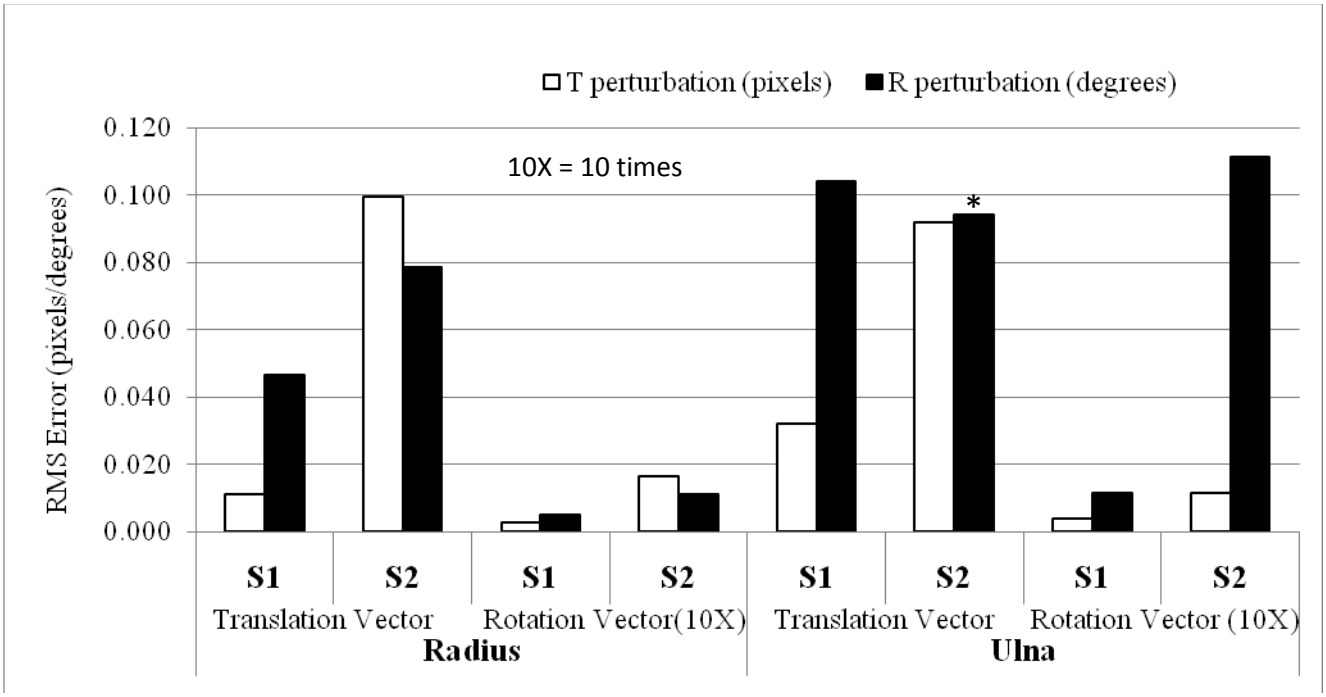

Figure 2.1 Comparison of the RMS errors averaged over perturbation level and direction for radius and ulna due to translation T (pixels) and rotation R (degrees) perturbations. Note that the scale for rotation is magnified by 10 times. *Ulna translation error for rotation perturbation of S2 only is divided by 10 on the chart.

RMS errors in translation vectors averaged over perturbation level and both radius and ulna were observed to be higher for rotation perturbations of S1 and translation perturbations of S2 but had no specific trend with regard to direction (Fig 2.2). Similar observations were also made for RMS errors in translation vectors averaged over each direction (Fig 2.4). Translation and rotation perturbations in S2 caused higher errors in the attitude (rotation) vector of S2 when compared to S1 (Fig 2.3 & Fig 2.5). There was no consistent trend in the errors according to

perturbation level or with respect to direction. Errors for S2 were consistently higher than errors for S1. Both radius and ulna exhibited higher absolute errors due to rotation perturbations for S1. For S2, both the radius and ulna exhibited higher absolute errors due to translation perturbations.

The amount of error for a 1 pixel translation perturbation and a 3 pixel translation perturbation were observed to be nearly the same magnitude (Fig 2.4-2.5).

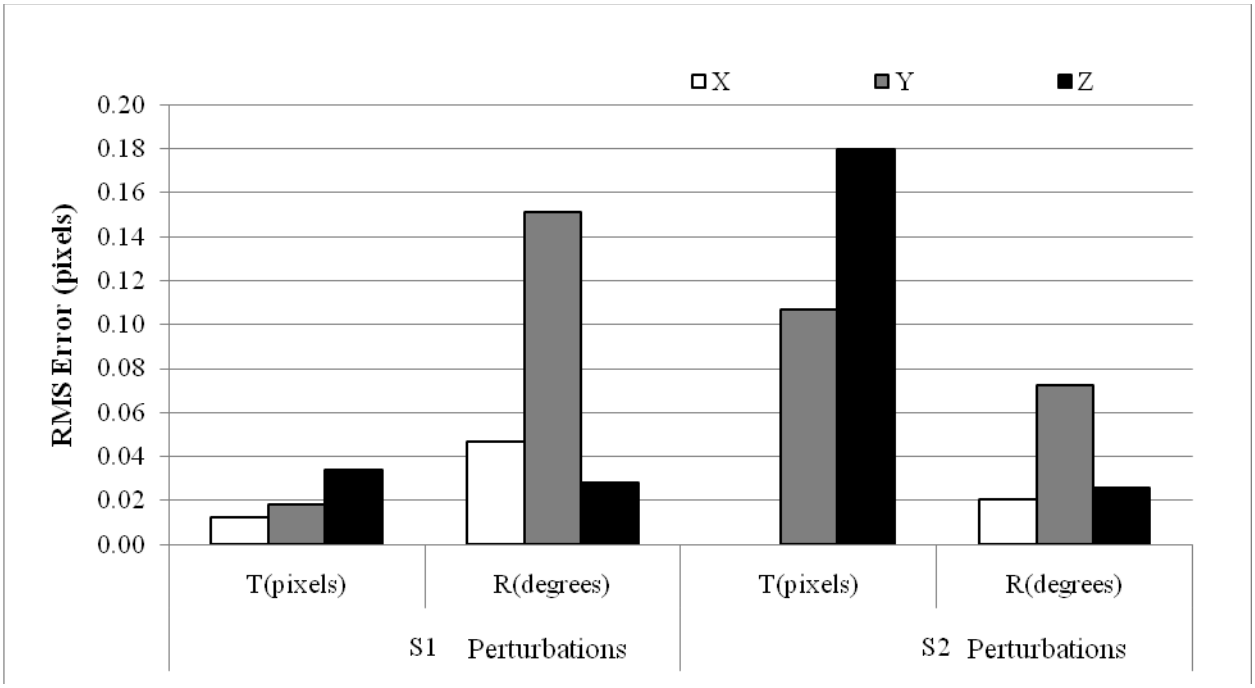

Figure 2.2 Comparison of the RMS errors in translation vector averaged over perturbation level and both radius and ulna for translation perturbations T (pixels) and rotation perturbations R (degrees) for X, Y, Z directions

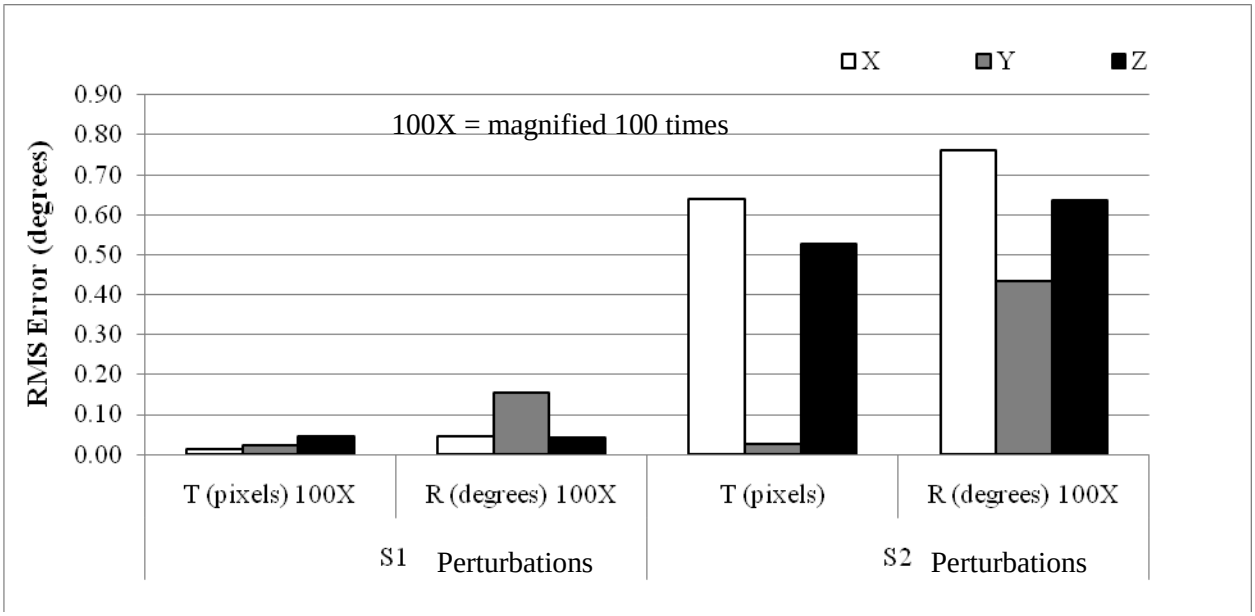

Figure 2.3 Comparisons of the RMS errors in rotation vector averaged over perturbation level and both radius and ulna for translation perturbations T (pixels) and rotation perturbations R (degrees) for the X, Y, Z directions

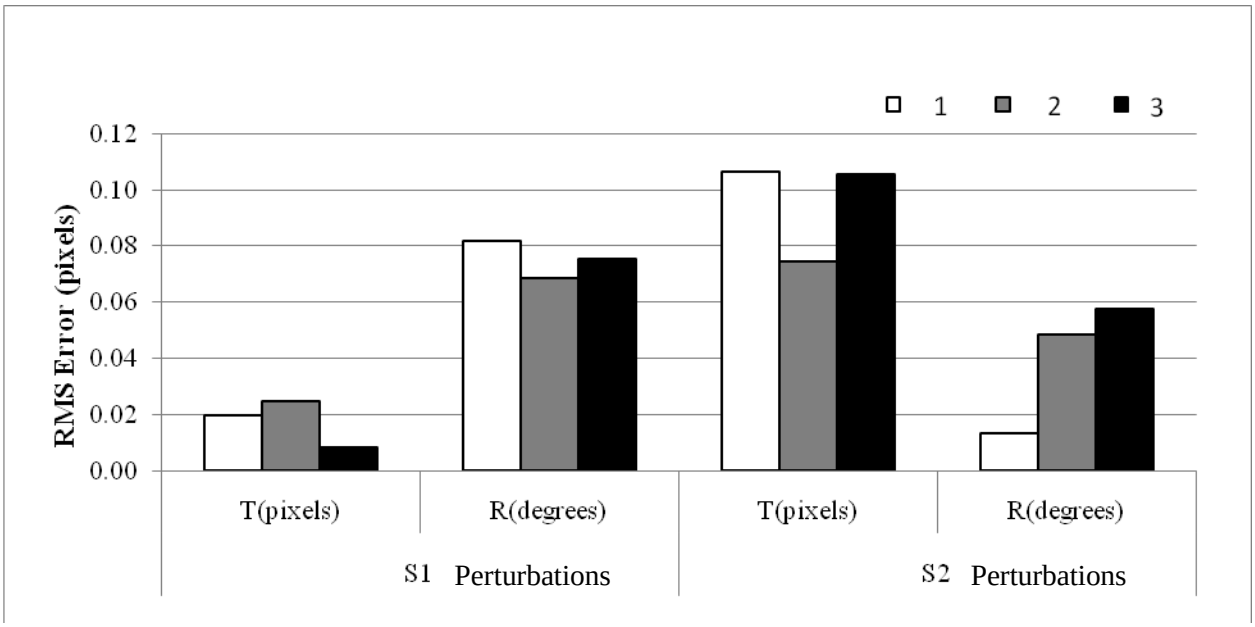

Figure 2.4 Comparison of the RMS errors in translation vector averaged over each direction and both radius and ulna of translation T (pixels) and rotation R (degrees) perturbations for 1, 2& 3 pixels/degrees of perturbations

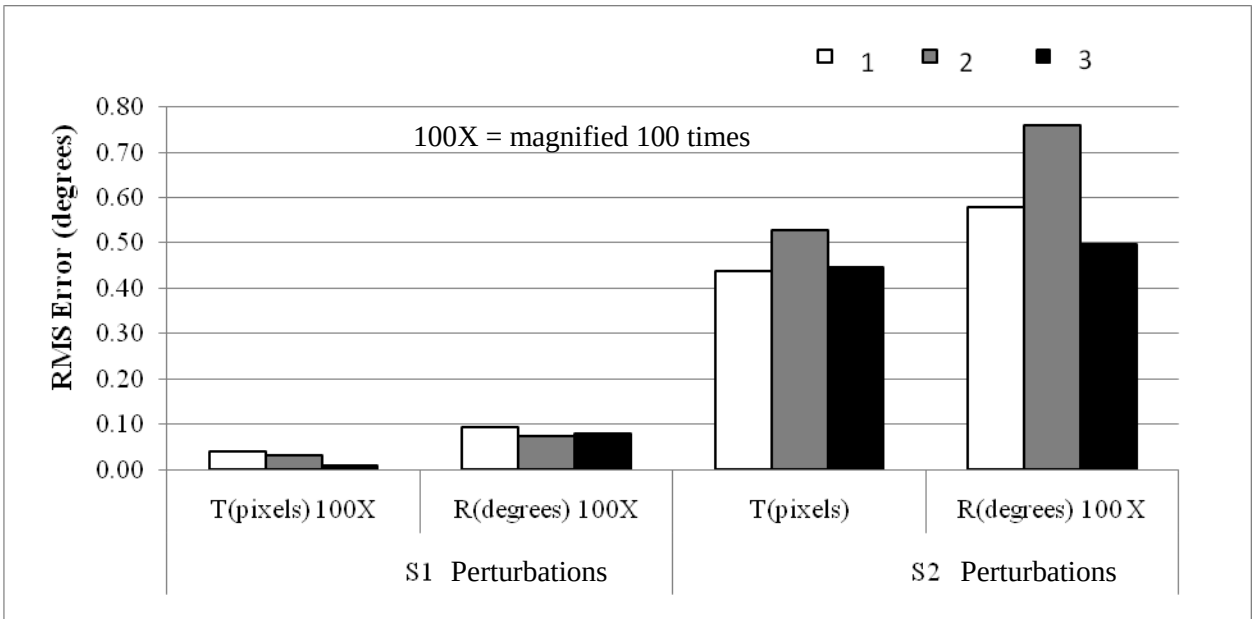

Figure 2.5 Comparison of the RMS errors in rotation vector averaged over each direction and both radius and ulna for translation T (pixels) and rotation R (degrees) perturbations of 1, 2 & 3 pixels/degrees of perturbations

2.4. Discussion and Conclusions

In this study we evaluated the effect of perturbations from the manual registration initial conditions on the final registration transformations of bones in the distal radioulnar joint. The effect of the differences in imaging plane on the accuracy of the final registration was investigated as a part of this study. In general, the results show that the ulna rotation in image set of S2 resulted in greater kinematic differences due to perturbations. This emphasizes the need for consistent forearm and wrist position when imaging for kinematic analysis.

Goto et al [73] did an in vivo 3-D wrist motion analysis using MR imaging and volume based registration. He found that volume based registration is likely to be less sensitive to the segmentation errors than surface based registration. Their study also found that the kinematics of the carpal bones were affected by the shape of the bone. The finding was supported by the study

of Crisco et al. [53], who found larger errors for lunate than for scaphoid and capitate due to its smaller size and more spherical shape.

From the findings in this study it was observed that the errors trended higher for translation perturbations in S2 compared to rotation perturbations in S2. Translation perturbations generally result in larger errors than rotation perturbations for S2. It can be concluded that imaging different forearm positions or using different imaging planes leads to greater registration/kinematic errors. This emphasizes the need to be as consistent as possible in forearm position and/or imaging plane. It can also be concluded that small errors in manual registration will not generally have a great affect on the final registration. While the results presented were from only two subjects, they indicate the importance of careful imaging and registration techniques for the most accurate results.

2.5. Acknowledgements

We would like to acknowledge funding from National Institutes of Health (NIH) and Allan Schmitt for technical assistance in imaging.

3. *In vivo* contact mechanics of the distal radioulnar joint (DRUJ)

3.1. Introduction

The Distal radioulnar joint (DRUJ) is a joint of the wrist which allows the forearm rotation and force transmission in the upper limb while preserving stability independent of flexion and extension of the elbow or wrist [3, 4, 7, 8, 10, 23]. The triangular fibro cartilage complex (TFCC) which is comprised of the various soft tissue structures and the interosseous membrane of the forearm provide major stability to the joint [3, 23, 64, 114-116]. Disruption of any of these elements or bony trauma may lead to instability, loss of motion, and even arthrosis of the DRUJ [3, 64].

DRUJ may be injured either in isolation [43, 117] or in association with a nearby wrist injury [22, 23, 64]. Distal radial fracture is the most common wrist injury which affects the mechanics of the DRUJ [118], leading to conditions such as positive ulnar variance (ulnar impaction syndrome) [34] or negative ulnar variance (ulnar impingement) [34, 40, 119] or other ulnar sided wrist pain [22, 23, 41, 120]. Studies have shown that the presence of intra articular fracture of the distal radius can lead to the development of premature arthritis of the DRUJ [121, 122]. The mechanics of the DRUJ can also be affected by the instability of the carpal bones [33, 123].

Scapholunate dissociation (SLD) is a serious carpal ligamentous injury to the wrist caused by the rupture of the scapholunate ligament. SLD results in rotary sublaxations and dissociation of scaphoid from lunate. These abnormal motions create excessive stress and shear loading of articular surfaces leading to degenerative arthritis [42, 124]. Czitrom et al. [33] and others found a significant correlation between negative ulnar variance and recent scapholunate

dissociation [123]. De Smet et al. [125] contradicted this by stating that ulnar variance has no importance in scapholunate dissociations. Changes in ulnar variance results in significant changes in the biomechanical forces of the wrist [126]. An increase in ulnar length would result in reducing the strain on the lunate but increasing the contact forces borne by the distal ulna leading to the degeneration of TFCC [12, 125]. It is vital to find out whether or not scapholunate dissociation causes changes in the radioulnar joint mechanics, as altered joint mechanics are highly associated with onset of OA [1]. An understanding of the normal and pathological *in vivo* DRUJ mechanics should help physicians make better clinical recommendations and improve treatment for the primary injury and its associated pathology.

Various researchers have investigated the load transfer characteristics of the DRUJ and wrist in vitro by evaluating the force transmission [12, 51, 57, 58, 127-132] and contact pressure using films and sensors [6, 20, 52, 60, 133, 134]. With advancement in technology, imaging techniques such as computed tomography (CT) [135, 136] and magnetic resonance (MR) imaging [135-137] have been used extensively to evaluate the wrist joint and the DRUJ *in vivo* with various modeling techniques.

The overall goal of the research program is to characterize normal and pathological wrist mechanics during functional loading, to evaluate the surgical repair, and to relate any changes with pathology to onset of OA. The objective of this study was to evaluate the contact mechanics of the DRUJ with unilateral scapholunate dissociation and in contralateral normal wrists based on MRI scans during functional loading coupled with surface contact modeling [101]. In addition, DRUJ mechanics were also evaluated in surgically repaired wrists. It was hypothesized that peak contact pressures and contact areas would be higher for injured wrist than for the normal and surgically repaired wrists.

3.2. Methods

Six human subjects with unilateral scapholunate dissociation and no known wrist arthritis participated in this study. The Human subjects Committee of the University of Kansas Medical Center approved the human subject protocol. All the subjects were screened for contralateral wrist injury prior to participation. The uninjured wrist served as a subject specific normal contralateral control joint and made possible the comparison between normal and injured wrists. The MR imaging was done in the Hoglund Brain Imaging center on the University of Kansas Medical Center campus. The scans were performed on a 3T MRI scanner (Allegra, Magnetom Vision Plus, Siemens, Malvern, PA) with a custom made double loop surface coil placed on the wrist and using a constructive interference steady state (CISS) pulse sequence. For all the subjects, two scans were performed for each wrist, one with the hand relaxed and the second one during active light grasp with scan times of about 12 minutes and 3 minutes, respectively. The injured wrist was first scanned with the hand relaxed with a slice thickness of 0.5 mm and an in-plane pixel size of 0.15 mm. A second scan was taken during active light grasp with a slice thickness of 1.0 mm and a pixel size of 0.3 mm. The subjects wore wrist braces to ensure consistent wrist position during the light grasp scans. The subjects maintained a constant grip pressure during the active grasp scan using a visual feedback system. The visual feedback system consists of a MRI compatible pneumatic pressure section, remote transducer which reads the pressure applied and fiber optic computer display head set which displays the pressure in real time allowing the subjects to maintain constant pressure. This procedure was repeated for the contralateral normal wrists and for the injured wrists post-operatively.

The high resolution images obtained from the relaxed scans were used to construct models of the distal radius and ulna, including cartilage. The images were segmented using

MPXImage, custom software (Manson, University of Pittsburgh, 1998). Due to image quality, segmentation was performed manually utilizing editable bezier spline overlays that produced a smooth contour of the bone. The output of the segmentation, a structured 3D point cloud was then imported into Geomagic Studio 9.0 (Raindrop Geomagic, Research Triangle Park, NC) which was used to wrap the point cloud with triangular faceted surfaces, defining the bone geometry. These surface models were formatted for the analysis in the Joint_Model program.

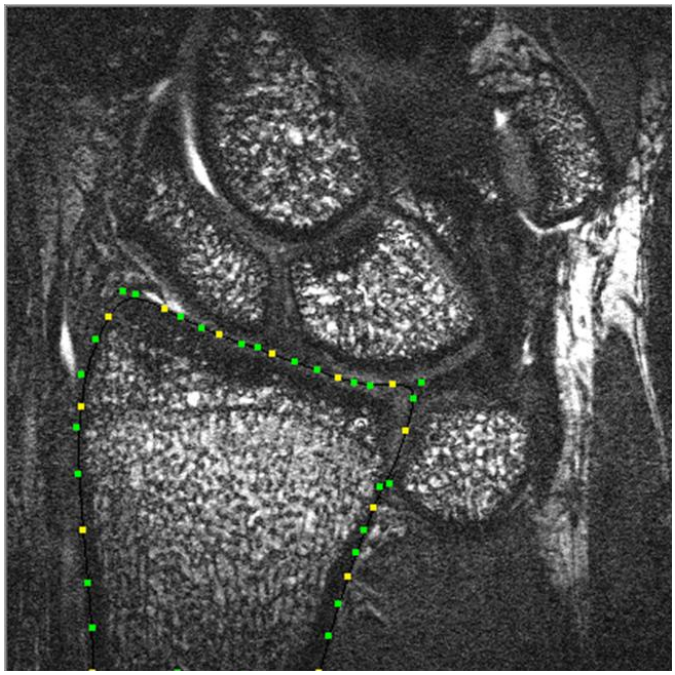

Figure 3.1 Example of the segmentation procedure used for making geometric models

Both unloaded and loaded image sets were also isolated with Adobe Photoshop Elements (Adobe Systems, San Jose, CA, USA) to separate radius and ulna individually on a black background for individual bone image registration. These registrations were performed to determine model kinematics from unloaded to loaded configuration. Image registration was performed using Analyze 5.0 (Analyze Direct, Overland Park, KS) with a combination of manual and auto 3D voxel registrations to obtain a best fit.

Kinematic analysis involved two transformations. The kinematic analysis was performed with a basic assumption that the bones deform negligibly during light grasp loads. For this study, the radius was selected as the reference (fixed) bone with the ulna moving relative to it. First, the loaded radius was registered to the unloaded radius, to determine the kinematic transformation from the loaded to the unloaded coordinate system. This transformation was used to transfer the loaded ulna image set to the unloaded coordinate system. Second, the unloaded ulna was registered to match the transformed loaded ulna to give a final transformation for the unloaded model to reach the loaded configuration. The translations and rotations were applied to the surface geometry models with cartilage in the Joint_Model software.

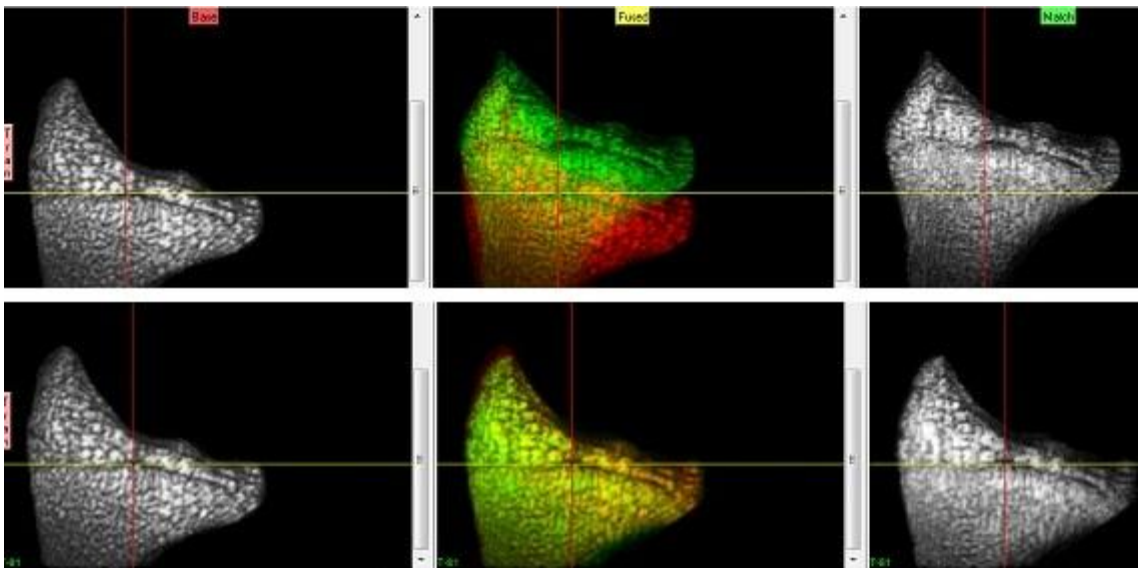

Figure 3.2 Radius registration in Analyze. Left shows the unloaded radius volume and the right shows the loaded isolated radius volume

The contact mechanics analysis was performed using the surface models in the program Joint_Model software [2]. The kinematics obtained from registration placed the models in functionally loaded state in this program. Joint_Model program assumed the bodies to be undeformable and determined the contact pressure from the interpenetration of the body surfaces based on a defined contact rule. The defined contact rule gave the first order estimate of cartilage

strain based on the thickness of the cartilage on each bone and depth of interpenetration (overclosure) of the bodies in contact, from the geometry and loaded configurations of the surface models. The contact rule also specified the contact pressure to be directly proportional to the interpenetration of the model surfaces. For all the bone models, the cartilage was assigned a uniform thickness (1 mm) and an effective cartilage relaxation modulus (4MPa). The program used the kinematics and the contact rule to determine the contact mechanics for the distal radioulnar joint. The Joint_Model program provided contact area, peak contact pressure and contact force for the DRUJ. The overall region of interpenetration directly gives the contact area. The local contact pressures are calculated by the level of interpenetration and the material properties. Contact pressure integrated over the contact area yields the total contact force of the articulation. Average pressure was calculated as the ratio of the contact force and the contact area.

To verify the accuracy of the model data from the human subjects, contact area was calculated directly from the apparent contact on each image of the grasp MRI scans. The curve of contact of the joint was carefully segmented on each image and length of arc was calculated. The length of arc multiplied by slice thickness of each image gave the contact area from each image and the summation of contact area of all images gave the total contact area. The contact areas measured directly from the MR images were compared with the contact areas obtained from the corresponding models.

Model contact parameters from the injured wrist were compared with those from the contralateral normal wrists and the injured wrist post operatively (n=2) using ANOVA with Fisher's PLSD post-hoc analysis. Paired t-test was used to compare the contact parameters from the injured wrist (n=5) with those of the contralateral normal wrist (n=5). A significance level of

$p<0.05$ was defined for both the analyses. A repeatability test was performed for one subject to test the repeatability between two separate analyses.

3.3. Results

Table 3.1 summarizes the contact parameters obtained from the surface model contact analysis of the DRUJ.

3.1 Model contact data and direct MR image contact area measurements for Normal and Injured wrists for subject 1 (S1), subject 2 (S2), subject 3 (S3), subject 4 (S4), subject 5 (S5), subject 6 (S6) and Repaired wrists (S1, S3).

Subject No.	Condition	Radioulnar				
		Force (N)	*PP (MPa)*	*AP (MPa)*	*Area (mm^2)*	*Direct Area (mm^2)*
S1	**Normal**	20.3	1.0	0.45	45.4	43.9
	Injured	20.0	1.2	0.43	46.6	50.3
	Repaired	11.7	0.9	0.37	31.7	33.4
S2	**Normal**	1.0	0.3	0.12	8.0	10.0
	Injured	2.6	1.3	0.75	3.5	3.1
S3	**Normal**	1.0	0.4	0.23	4.2	19.7
	Injured	3.2	0.6	0.28	11.4	14.6
	Repaired	7.4	1.8	0.63	11.9	22.0
S4	**Normal**	8.5	1.1	0.32	27.0	27.5
	Injured	39.4	1.9	1.07	36.7	38.2
S5	**Normal**	7.2	1.0	0.46	15.6	10.8
	Injured	5.4	0.62	0.30	17.6	18.0
S6	**Normal**	0.0	0.0	0.00	0.0	19.8
	Injured	6.0	1.0	0.47	12.8	30.4

Qualitatively, the contact pattern on the radius fossa is different for each of the normal, injured and the repaired wrists for each subject. There was a dorsal shift in the ulnar contact with the radius in the injured wrist compared to the normal. This contact shifted back to near normal position after the surgery (Fig 3.3).

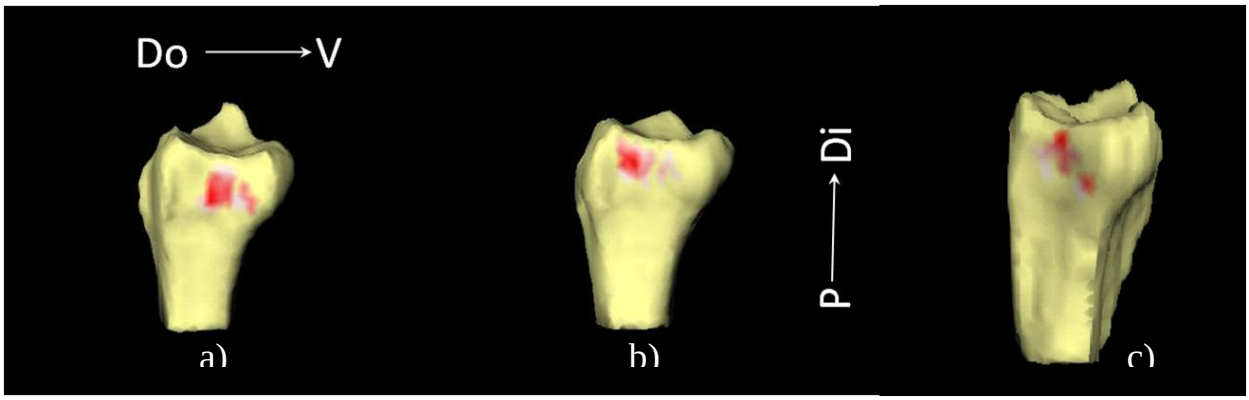

Figure 3.3. a) Normal (left) vs. b) injured (right) vs c) repaired wrist contact pressure patterns for ulnar contact shown on radius fossa for Subject 1 (S1). (Do-Dorsal; V-Volar; P-Proximal; Di-Distal)

Contact forces (Mean ± Std Dev.) for the radioulnar articulation were 7.59 ± 7.89 and 14.12 ± 15.86 N for the normal and injured wrists (n=5), respectively, and 9.6 ± 3.0 N for repaired wrists (n=2) (Fig 3.4). The contact forces showed an increasing trend from the normal to the injured wrists in all subjects, except S1 and S5 that decreased slightly. The repaired wrists had lower force in S1 than the injured wrists, whereas DRUJ contact force was somewhat higher in the repaired wrist of S3 (Table 3.1).

Peak contact pressures (Mean ± Std Dev) for the radioulnar articulation were 0.74 ± 0.4, 1.15 ± 0.56, 1.38 ± 0.63 MPa for the normal wrists (n=5) and injured wrists (n=5) and repaired wrists (n=2), respectively (Fig. 3.5). Maximum peak contact pressure for the normal wrist was under 1.15 MPa, whereas, the maximum pressure in the injured wrist was 1.94 MPa. The radioulnar contact pressures tended to have higher values for the injured wrists but this was not significant (p=0.089).

Average contact pressures for the radioulnar contact were 0.32 ±0.14 MPa for the normal wrist, 0.57±0.34 MPa for the injured wrist and 0.50±0.18 MPa for the repaired wrists (Fig. 3.5). Each subject followed a unique progression of average contact pressure in the DRUJ. However,

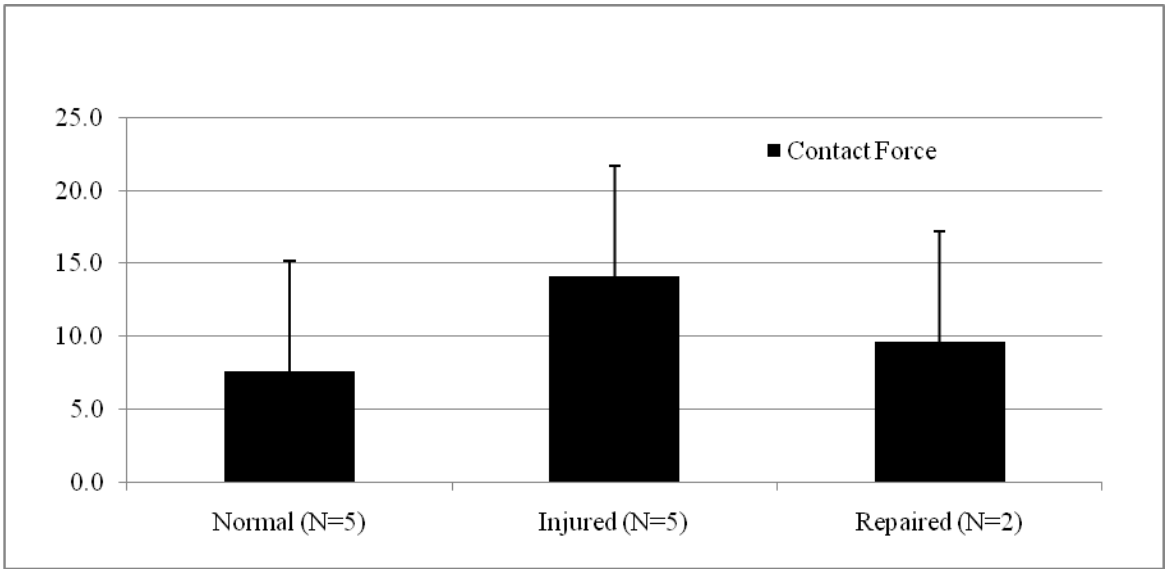

Figure 3.4 Comparison of the means of contact forces for Normal (N=5), Injured (N=5) and Repaired (N=2) wrists

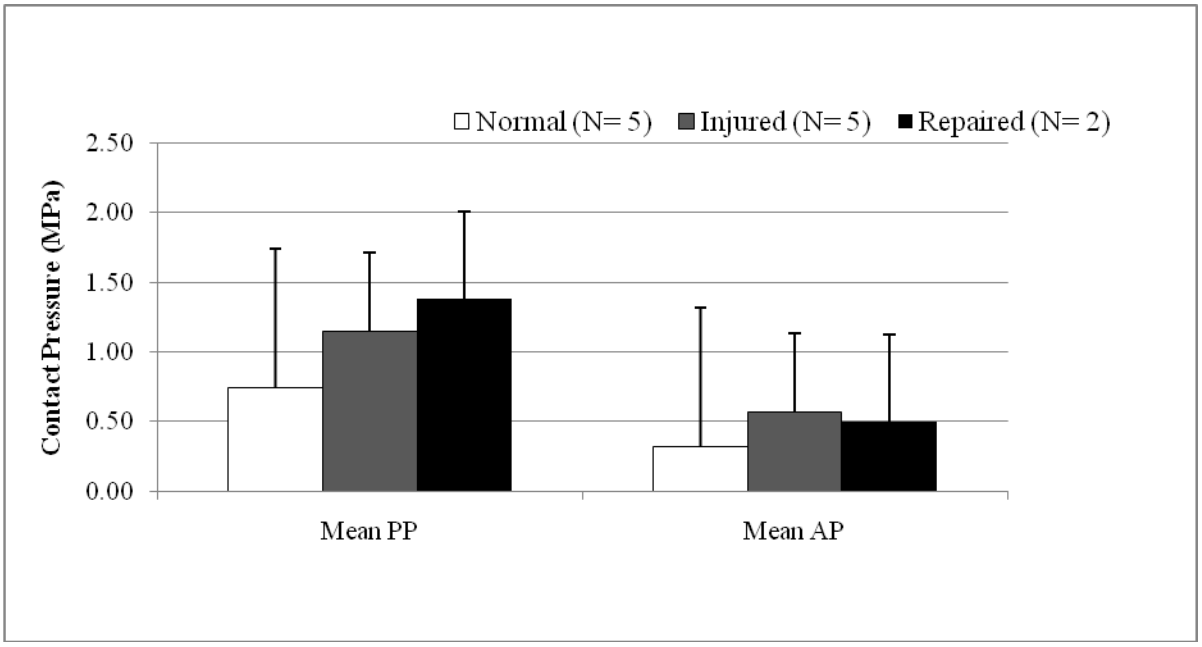

Figure 3.5 Comparison of the means of peak contact pressures (PP) and Average pressures for Normal (N=5), Injured (N=5) and Repaired wrists (N=2).

average pressures tended to be higher in the injured wrist than in normal wrists. The average pressures were reduced towards near normal after the surgery (Fig 3.5).

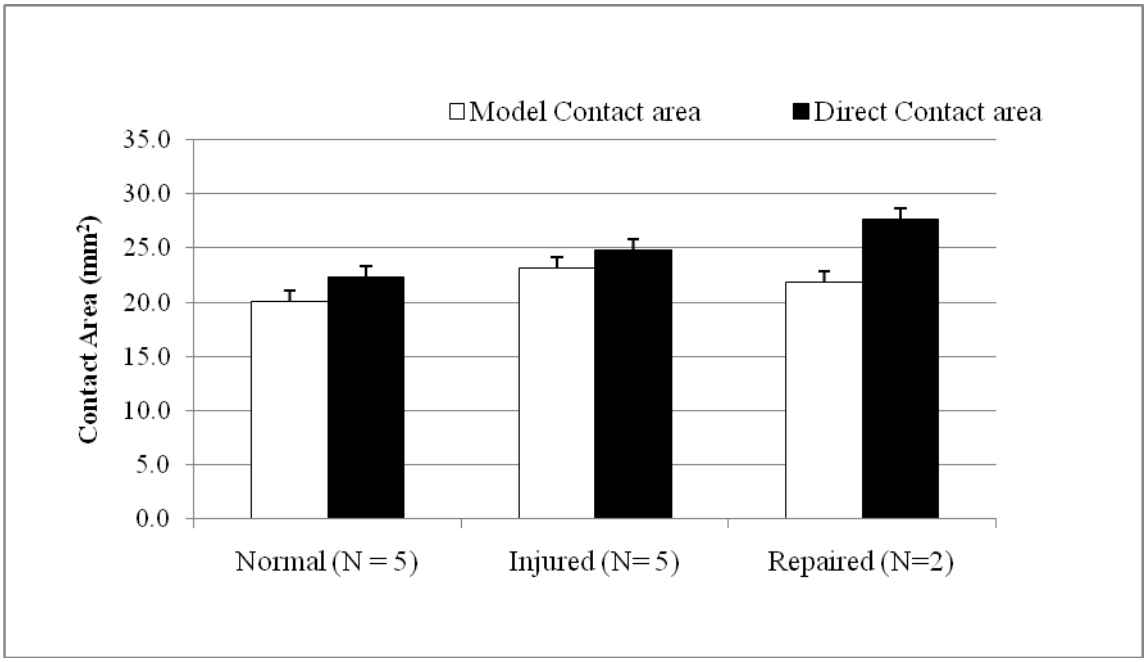

Figure 3.6 Comparison of contact area for Radioulnar (RU) contact calculated from the MRI based models and calculated directly from the grasp images for Normal (N=5), Injured (N=5) and Repaired (N=2) wrists

DRUJ model contact areas were 20.0 ± 16.6 mm^2 for the normal wrists, 23.1 ±18.0 mm^2 for the injured wrists and 21.8 ±14.0 mm^2 for the repaired wrists (Fig 3.6). A comparison was made between the contact areas determined from the contact model and from the area calculated directly from the MRI images. A maximum of 20% difference was seen in S2 normal between the model contact area and the directly measured contact area. The normal wrists for S3 and S5 each had an absolute difference of approximately 15 mm^2 between the model and direct contact areas. The average contact area calculated from the model was within 12% of the average of the direct MRI measurement for the normal wrists, 7% for the injured wrists, and 20% for the repaired wrists.

A paired T-test was done for all the contact parameters between normal (n=5) and injured (n=5) wrists. Repeated measures ANOVA was used for the statistical analysis of all the contact parameters of normal, injured and surgically repaired wrists (n=2). No significant

differences were found in either of the statistic analyses. This may be due to the low number of subjects, especially in the repair group.

Repeatability test

Table 3.2 shows the comparison of the contact parameters of the analysis for both the normal and the injured wrists in tests trial 1 (T1) and trial 2 (T2).

3.2 Contact parameters obtained in the analysis in trial 1 (T1) and trial 2 (T2) and the third row shows the absolute difference between the two trials of the repeatability test

Condition	Test	Radioulnar				
		Force (N)	*PP (MPa)*	*AP (MPa)*	*Area (mm^2)*	*Direct Area (mm^2)*
Normal	**T1**	4.43	0.87	0.59	7.50	7.69
	T2	7.24	0.97	0.46	15.57	10.75
	Difference	**2.81**	**0.10**	**-0.13**	**8.07**	**3.06**
Injured	**T1**	3.79	0.36	0.22	17.55	20.73
	T2	5.35	0.62	0.30	17.57	18.01
	Difference	**1.56**	**0.26**	**0.09**	**0.02**	**-2.72**

Repeatability between the two separate analyses was generally quite good. Absolute differences in contact forces were less than 3N. Peak contact pressures were within 0.3 MPa, and average contact pressures were within 0.15 MPa. Model contact area was within 8 mm2 and matched directly measured contact area closely.

3.4. Discussion

The results indicated possible changes in the DRUJ joint mechanics with scapholunate dissociation injury. The DRUJ is a complex joint due to many soft tissues structures that interact with it, and MRI based modeling was very helpful in analyzing the joint in human subjects non-invasively. The accuracy of these models was dependent on the image quality, which was

reduced in some cases due to motion artifact and the positioning of the transmit/receive MRI coil that reduced signal from the ulna.

The peak contact pressures in this study were found to be less than 2MPa which can be consistent with a previous ex vivo study where the maximum peak pressure in the wrist joint was found to be less than 3 MPa [138]. These values can be further supported by another ex vivo study on DRUJ by Nishiwaki and his group in which they observed a peak pressure of 1.04 MPa [139]. The peak pressure generally trended to higher values in the injured wrists when compared to the normal wrists and the surgically repaired wrists. Average contact pressures also generally showed an increasing trend from the normal wrists to the injured wrists and reduced to near normal values in the repaired wrists.

Similarly, contact force in the DRUJ for the radioulnar articulation for the injured wrists generally tended to be higher in the injured wrists than in the normal and the surgically repaired wrists. The forces for the subjects were less than 20 N except for two subjects in which forces were approximately 40 N. In an ex vivo study, the forces transmitted through the DRUJ were found to be less than 10N in the loaded condition in a normal wrist under an external load of 20N [139]. Shabaan and his coworkers investigated the force transmission through DRUJ in cadaveric specimens in various forearm positions and concluded that force transmitted across the DRUJ changes with sequential loading to the hand and forearm. This may be one of the reasons for the wide range of contact force values we observed in our study. They also found that force transmitted across the radius and ulna was higher in supination than pronation and our subjects were generally scanned in supination [51]. Although, none of these parameters were statistically significant, they provide some evidence that wrist injury may lead to changes at the DRUJ of the wrist and might increase the risk of OA in the joint.

The location of contact of the DRUJ articulation on the radius shifted dorsally for the injured wrists compared to the normal wrists. Af Ekenstam et al [140] investigated the DRUJ force transmission and found the contact area and force transmission across the DRUJ differing throughout the arc of rotation of the forearm[140]. The rotatory movement of the radius around a relatively stable ulna head is accompanied with translation and the contact shifts from dorsal in sigmoid notch in pronation to volar in supination [115]. Most of our analyses are for wrist in supination. The contact location shifts from volar to dorsal position when the elbow changes from flexion to extension. It was confirmed in another study by Shabaan and his research group that the contact area changes predictably with axial loading of the hand and rotation of the forearm [139].

Contact area of the normal, injured and the surgically repaired wrists was found to be less than 20 mm^2 in most of the wrists. Previous ex vivo studies have shown that the area of contact between the joint surface of the radius and ulna is relatively very small owing to the lower amount of force transmitted across the DRUJ [115, 139]. In a similar study made by Ishi and his co investigators using sensors, the contact area was found to be 7.6 mm^2 and 15.6 mm^2 in unloaded and loaded conditions respectively [52]. Nishiwaki et al found the contact area to be less than 11 mm^2 for different forearm positions in a cadaveric study [139]. Based on a study on effect of forearm rotation on grip strength, Shabaan et al also postulated that there is a relationship between joint contact areas and grip strength [141].

The contact area data in this in vivo study was verified by making a comparison of model contact area with contact measured directly from the grasp images. The model contact data and direct contact data were quite consistent suggesting the reliability of the modeling results.

This study is still preliminary and additional subjects would provide more conclusive evidence to evaluate the efficacy of the surgical repair in correcting the altered mechanics post operatively. Contact parameters especially contact force and peak pressures are highly dependent on the accuracy of surface model geometries and kinematics. Overall accuracy could be increased with improved quality of the images. The current data suggest that the scapholunate injury may alter the mechanics of the DRUJ. This study can also be further extended to analyze the effect of ulnar variance on the mechanics of articulation. Thereby, future studies may help provide potential recommendations for a careful assessment and improved treatment of injuries affecting the DRUJ.

3.5. Acknowledgements

We would like to acknowledge funding from NIH, Columbia University for use of Joint_Model software, Allan Schmitt for image acquisition, assistance from Mahender Mandala and Michael Humphrey with image processing.

4. Summary and Future Directions

The MRI based modeling approach used in these studies was validated on a radiocarpal joint in the wrist in cadaveric specimens. The results obtained from the current in vivo contact mechanics study of the DRUJ and perturbation studies illustrated the advantages and limitations of the MRI based contact modeling approach.

Six Human subjects were a part of the radioulnar mechanics. Models of radius and ulna were constructed from MR scans obtained using a 3 Tesla scanner and custom made coil. The images were acquired for both unloaded and loaded configurations for normal (n=5), injured (n=5) and surgically repaired wrists (n=2). Kinematics defining transformations from unloaded to loaded state were obtained and these were input in a contact modeling program for analysis. The contact forces showed an increasing trend from normal to the injured wrists. Similarly, peak contact pressures and average contact pressures also trended higher for injured wrists compared to normal wrists and reduced to near normal position after the surgery. The contact area location shifted dorsally in the injured wrists from the normal wrists and this indicates the change in the mechanics of the DRUJ due to the injury. This shift in the contact may also be due to the differences in forearm positions based on previous studies by Shabaan and Ishii et al. The contact areas of the normal, injured and the repaired wrists was found to be less than 20 mm^2 in most of the wrists.

Results obtained from this study were comparable to studies conducted in the past. Also direct measurement of contact area from MR images were found to be very close to model contact areas obtained from the analysis providing confidence in the MRI based modeling approach. The repeatability test between two separate analyses for a certain subject was generally quite good showing the reliability in the method.

The main concern with the models constructed from MR images is the quality of the images. For the most accurate geometric models, images should have high resolution and signal to noise ratio. Image quality also affected the kinematic analysis performed with image registration. The loaded images were acquired at half the resolution of unloaded images to minimize the grasp scan time. Thus, the resolution of loaded images could potentially lead to inaccurate kinematics which would help explain variations in the data and some of the discrepancies between contact model area measurements and direct MR area measurements.

A perturbation study was done to find the combined effect of the initial registration conditions and the imaging plane orientation on the final registration used for *in vivo* kinematic analysis of the distal radioulnar joint. Translation perturbations of 1, 2, 3 voxels and rotation perturbations of 1, 2, 3 degrees were applied to the standard manual registration along each of X, Y, Z directions individually. RMS errors of translation and attitude vectors were obtained comparing each of the perturbation best matches with the standard best match. Results indicated higher translation errors of the attitude vectors for both radius and ulna for Subject II compared to Subject I due to a different forearm position (image plane orientation) emphasizing the need to be careful while imaging to have a consistent forearm position and image plane orientation to increase the accuracy of the kinematic analysis.

The images used for this study were not focused on the radioulnar joint and had issues such as motion artifact and low signal (especially for ulna) for some subjects. This issue can be solved by using a larger coil with a better signal to noise ratio (SNR). It is also important to maintain a stable and consistent forearm position. While the present data shows that the scapholunate dissociation could alter the mechanics of the distal radioulnar joint, more affirmative conclusions

can be made by analyzing additional subjects especially post operatively. FE models can be used to obtain more accurate and in depth results characterizing stresses and strains during functional joint loading of the DRUJ.

5. References

1. Buckwalter, J.A., C. Saltzman, and T. Brown, *The impact of osteoarthritis: implications for research.* Clin Orthop Relat Res, 2004(427 Suppl): p. S6-15.
2. Kwak, S.D., L. Blankevoort, and G.A. Ateshian, *A Mathematical Formulation for 3D Quasi-Static Multibody Models of Diarthrodial Joints.* Comput Methods Biomech Biomed Engin, 2000. **3**(1): p. 41-64.
3. Drobner, W.S. and M.R. Hausman, *The distal radioulnar joint.* Hand Clin, 1992. **8**(4): p. 631-44.
4. Kapandji, A., *Biomechanics of pronation and supination of the forearm.* Hand Clin, 2001. **17**(1): p. 111-22, vii.
5. Kijima, Y. and S.F. Viegas, *Wrist anatomy and biomechanics.* J Hand Surg Am, 2009. **34**(8): p. 1555-63.
6. Schuind, F., et al., *Force and pressure transmission through the normal wrist. A theoretical two-dimensional study in the posteroanterior plane.* J Biomech, 1995. **28**(5): p. 587-601.
7. Linscheid, R.L., *Biomechanics of the distal radioulnar joint.* Clin Orthop Relat Res, 1992(275): p. 46-55.
8. Hagert, C.G., *Distal radius fracture and the distal radioulnar joint--anatomical considerations.* Handchir Mikrochir Plast Chir, 1994. **26**(1): p. 22-6.
9. Berger, R.A., *Arthroscopic anatomy of the wrist and distal radioulnar joint.* Hand Clin, 1999. **15**(3): p. 393-413, vii.
10. Palmer, A.K., *The distal radioulnar joint.* Orthop Clin North Am, 1984. **15**(2): p. 321-35.

11. Nicolaidis, S.C., D.H. Hildreth, and D.M. Lichtman, *Acute injuries of the distal radioulnar joint.* Hand Clin, 2000. **16**(3): p. 449-59.

12. Palmer, A.K. and F.W. Werner, *Biomechanics of the distal radioulnar joint.* Clin Orthop Relat Res, 1984(187): p. 26-35.

13. Patterson, R. and S.F. Viegas, *Biomechanics of the wrist.* J Hand Ther, 1995. **8**(2): p. 97-105.

14. Berger, R.A., *The anatomy of the ligaments of the wrist and distal radioulnar joints.* Clin Orthop Relat Res, 2001(383): p. 32-40.

15. Short, W.H., et al., *A biomechanical study of distal radial fractures.* J Hand Surg Am, 1987. **12**(4): p. 529-34.

16. Linscheid, R.L. and J.H. Dobyns, *Athletic injuries of the wrist.* Clin Orthop Relat Res, 1985(198): p. 141-51.

17. Moore, D.C., et al., *Three-dimensional in vivo kinematics of the distal radioulnar joint in malunited distal radius fractures.* J Hand Surg Am, 2002. **27**(2): p. 233-42.

18. Goldberg, H.D., et al., *Double injuries of the forearm: a common occurrence.* Radiology, 1992. **185**(1): p. 223-7.

19. Vesely, D.G., *The distal radio-ulnar joint.* Clin Orthop Relat Res, 1967. **51**: p. 75-91.

20. Bowers, W.H., *Instability of the distal radioulnar articulation.* Hand Clin, 1991. **7**(2): p. 311-27.

21. Bruckner, J.D., D.M. Lichtman, and A.H. Alexander, *Complex dislocations of the distal radioulnar joint. Recognition and management.* Clin Orthop Relat Res, 1992(275): p. 90-103.

22. Buterbaugh, G.A. and A.K. Palmer, *Fractures and dislocations of the distal radioulnar joint.* Hand Clin, 1988. **4**(3): p. 361-75.

23. Dell, P.C., *Traumatic disorders of the distal radioulnar joint.* Clin Sports Med, 1992. **11**(1): p. 141-59.

24. Bruckner, J.D., A.H. Alexander, and D.M. Lichtman, *Acute dislocations of the distal radioulnar joint.* Instr Course Lect, 1996. **45**: p. 27-36.

25. Glowacki, K., et al., *Disorders of the distal radioulnar joint.* Am J Orthop (Belle Mead NJ), 1997. **26**(3): p. 193-200.

26. Stoffelen, D., L. De Smet, and P. Broos, *The importance of the distal radioulnar joint in distal radial fractures.* J Hand Surg Br, 1998. **23**(4): p. 507-11.

27. Dyer, C.R., S.H. Kuschner, and W.W. Brien, *The distal radioulnar joint following Galeazzi's fracture.* Orthop Rev, 1994. **23**(7): p. 587-92.

28. Rettig, M.E., et al., *Wrist fractures in the athlete. Distal radius and carpal fractures.* Clin Sports Med, 1998. **17**(3): p. 469-89.

29. Nakamura, R., et al., *The influence of age and sex on ulnar variance.* J Hand Surg Br, 1991. **16**(1): p. 84-8.

30. Palmer, A.K., R.R. Glisson, and F.W. Werner, *Ulnar variance determination.* J Hand Surg Am, 1982. **7**(4): p. 376-9.

31. Epner, R.A., W.H. Bowers, and W.B. Guilford, *Ulnar variance--the effect of wrist positioning and roentgen filming technique.* J Hand Surg Am, 1982. **7**(3): p. 298-305.

32. Kristensen, S.S. and K. Soballe, *Kienbock's disease--the influence of arthrosis on ulnar variance measurements.* J Hand Surg Br, 1987. **12**(3): p. 301-5.

33. Czitrom, A.A., J.H. Dobyns, and R.L. Linscheid, *Ulnar variance in carpal instability.* J Hand Surg Am, 1987. **12**(2): p. 205-8.

34. Tomaino, M.M., *Ulnar impaction syndrome in the ulnar negative and neutral wrist. Diagnosis and pathoanatomy.* J Hand Surg Br, 1998. **23**(6): p. 754-7.

35. LaStayo, P. and S. Weiss, *The GRIT: a quantitative measure of ulnar impaction syndrome.* J Hand Ther, 2001. **14**(3): p. 173-9.

36. MacDermid, J.C., J.H. Roth, and R.S. Richards, *Pain and disability reported in the year following a distal radius fracture: a cohort study.* BMC Musculoskelet Disord, 2003. **4**: p. 24.

37. Steinborn, M., et al., *MR imaging of ulnocarpal impaction after fracture of the distal radius.* AJR Am J Roentgenol, 2003. **181**(1): p. 195-8.

38. Tatebe, M., et al., *Ulnocarpal impaction syndrome restricts even midcarpal range of motion.* Hand Surg, 2005. **10**(1): p. 23-7.

39. Friedman, S.L. and A.K. Palmer, *The ulnar impaction syndrome.* Hand Clin, 1991. **7**(2): p. 295-310.

40. Bell, M.J., R.J. Hill, and R.Y. McMurtry, *Ulnar impingement syndrome.* J Bone Joint Surg Br, 1985. **67**(1): p. 126-9.

41. Cerezal, L., F. del Pinal, and F. Abascal, *MR imaging findings in ulnar-sided wrist impaction syndromes.* Magn Reson Imaging Clin N Am, 2004. **12**(2): p. 281-99, vi.

42. Atkinson, L.S. and E.G. Baxley, *Scapholunate dissociation.* Am Fam Physician, 1994. **49**(8): p. 1845-50.

43. Lindau, T., et al., *Distal radioulnar instability is an independent worsening factor in distal radial fractures.* Clin Orthop Relat Res, 2000(376): p. 229-35.

44. Meldon, S.W. and S.W. Hargarten, *Ligamentous injuries of the wrist.* J Emerg Med, 1995. **13**(2): p. 217-25.

45. Brunelli, G.A. and G.R. Brunelli, *A new surgical technique for carpal instability with scapholunate dissociation.* Surg Technol Int, 1996. **5**: p. 370-4.

46. Hardy, P.A., P. Nammalwar, and S. Kuo, *Measuring the thickness of articular cartilage from MR images.* J Magn Reson Imaging, 2001. **13**(1): p. 120-6.

47. Weiler, P.J. and E.R. Bogoch, *Kinematics of the distal radioulnar joint in rheumatoid arthritis: an in vivo study using centrode analysis.* J Hand Surg Am, 1995. **20**(6): p. 937-43.

48. Catalano, L.W., 3rd, O.A. Barron, and S.Z. Glickel, *Assessment of articular displacement of distal radius fractures.* Clin Orthop Relat Res, 2004(423): p. 79-84.

49. Palmer, A.K., R.R. Glisson, and F.W. Werner, *Relationship between ulnar variance and triangular fibrocartilage complex thickness.* J Hand Surg Am, 1984. **9**(5): p. 681-2.

50. Moriya, T., et al., *Effect of triangular ligament tears on distal radioulnar joint instability and evaluation of three clinical tests: a biomechanical study.* J Hand Surg Eur Vol, 2009. **34**(2): p. 219-23.

51. Shaaban, H., et al., *The distal radioulnar joint as a load-bearing mechanism--a biomechanical study.* J Hand Surg Am, 2004. **29**(1): p. 85-95.

52. Ishii, S., et al., *Pressure distribution in the distal radioulnar joint.* J Hand Surg Am, 1998. **23**(5): p. 909-13.

53. Crisco, J.J., R.D. McGovern, and S.W. Wolfe, *Noninvasive technique for measuring in vivo three-dimensional carpal bone kinematics.* J Orthop Res, 1999. **17**(1): p. 96-100.

54. Genda, E., Horii, E., *Theoretical stress analysis in wrist joint--neutral position and functional position.* Journal of Hand Surgery (Edinburgh, Scotland), 2000. **25**(3): p. 292-5.

55. de Bruijn, H.P., *Functional treatment of Colles fracture.* Acta Orthop Scand Suppl, 1987. **223**: p. 1-95.

56. Jupiter, J.B., J. Ruder, and D.A. Roth, *Computer-generated bone models in the planning of osteotomy of multidirectional distal radius malunions.* J Hand Surg Am, 1992. **17**(3): p. 406-15.

57. af Ekenstam, F.W., A.K. Palmer, and R.R. Glisson, *The load on the radius and ulna in different positions of the wrist and forearm. A cadaver study.* Acta Orthop Scand, 1984. **55**(3): p. 363-5.

58. Werner, F.W., et al., *Force transmission through the distal radioulnar carpal joint: effect of ulnar lengthening and shortening.* Handchir Mikrochir Plast Chir, 1986. **18**(5): p. 304-8.

59. Viegas, S.F., et al., *Effects of radioulnar instability on the radiocarpal joint: a biomechanical study.* J Hand Surg Am, 1990. **15**(5): p. 728-32.

60. Werner, F.W., D.J. Murphy, and A.K. Palmer, *Pressures in the distal radioulnar joint: effect of surgical procedures used for Kienbock's disease.* J Orthop Res, 1989. **7**(3): p. 445-50.

61. King, G.J., et al., *Kinematics of the distal radioulnar joint.* J Hand Surg Am, 1986. **11**(6): p. 798-804.

62. Moojen, T.M., et al., *In vivo analysis of carpal kinematics and comparative review of the literature.* J Hand Surg Am, 2003. **28**(1): p. 81-7.

63. Mirarchi, A.J., et al., *Cadaveric biomechanical analysis of the distal radioulnar joint: influence of wrist isolation on accurate measurement and the effect of ulnar styloid fracture on stability.* J Hand Surg Am, 2008. **33**(5): p. 683-90.

64. Tsai, P.C. and N. Paksima, *The distal radioulnar joint.* Bull NYU Hosp Jt Dis, 2009. **67**(1): p. 90-6.

65. Moojen, T.M., et al., *Three-dimensional carpal kinematics in vivo.* Clin Biomech (Bristol, Avon), 2002. **17**(7): p. 506-14.

66. Neu, C.P., R.D. McGovern, and J.J. Crisco, *Kinematic accuracy of three surface registration methods in a three-dimensional wrist bone study.* J Biomech Eng, 2000. **122**(5): p. 528-33.

67. Crisco, J.J., et al., *Advances in the in vivo measurement of normal and abnormal carpal kinematics.* Orthop Clin North Am, 2001. **32**(2): p. 219-31, vii.

68. Crisco, J.J., et al., *Effects of distal radius malunion on distal radioulnar joint mechanics--an in vivo study.* J Orthop Res, 2007. **25**(4): p. 547-55.

69. Leonard, L., et al., *Development of an in-vivo method of wrist joint motion analysis.* Clin Biomech (Bristol, Avon), 2005. **20**(2): p. 166-71.

70. Sommer, H.J., 3rd and N.R. Miller, *A technique for kinematic modeling of anatomical joints.* J Biomech Eng, 1980. **102**(4): p. 311-7.

71. Patterson, R.M., et al., *High-speed, three-dimensional kinematic analysis of the normal wrist.* J Hand Surg Am, 1998. **23**(3): p. 446-53.

72. Kaufmann, R.A., et al., *Kinematics of the midcarpal and radiocarpal joint in flexion and extension: an in vitro study.* J Hand Surg Am, 2006. **31**(7): p. 1142-8.

73. Goto, A., et al., *In vivo three-dimensional wrist motion analysis using magnetic resonance imaging and volume-based registration.* J Orthop Res, 2005. **23**(4): p. 750-6.

74. Fischer, K.J., et al., *A method for measuring joint kinematics designed for accurate registration of kinematic data to models constructed from CT data.* J Biomech, 2001. **34**(3): p. 377-83.

75. Weiss, J.A. and J.C. Gardiner, *Computational modeling of ligament mechanics.* Crit Rev Biomed Eng, 2001. **29**(3): p. 303-71.

76. Fisk, J.P. and J.S. Wayne, *Development and validation of a computational musculoskeletal model of the elbow and forearm.* Ann Biomed Eng, 2009. **37**(4): p. 803-12.

77. Guess, T.M. and L.P. Maletsky, *Computational modeling of a dynamic knee simulator for reproduction of knee loading.* J Biomech Eng, 2005. **127**(7): p. 1216-21.

78. Liacouras, P.C. and J.S. Wayne, *Computational modeling to predict mechanical function of joints: application to the lower leg with simulation of two cadaver studies.* J Biomech Eng, 2007. **129**(6): p. 811-17.

79. Schmitt, R.R., *Imaging of the hand.* Eur J Radiol, 2011. **77**(2): p. 195.

80. Metz, V.M. and L.A. Gilula, *Imaging techniques for distal radius fractures and related injuries.* Orthop Clin North Am, 1993. **24**(2): p. 217-28.

81. Schreibman, K.L., et al., *Imaging of the hand and wrist.* Orthop Clin North Am, 1997. **28**(4): p. 537-82.

82. Wilson, A.J., F.A. Mann, and L.A. Gilula, *Imaging the hand and wrist.* J Hand Surg Br, 1990. **15**(2): p. 153-67.

83. Keir, P.J., *Magnetic resonance imaging as a research tool for biomechanical studies of the wrist.* Semin Musculoskelet Radiol, 2001. **5**(3): p. 241-50.

84. Zanetti, M., N. Saupe, and L. Nagy, *Role of MR imaging in chronic wrist pain.* Eur Radiol, 2007. **17**(4): p. 927-38.

85. Anderson, A.E., Ellis. B.J., Maas, S.A., *Validation of finite element predictions of cartilage contact pressure in the human hip joint.* J Biomech Eng, 2008. **130**(5): p. 051008.

86. Donahue, T.L., Hull, M.L., Rashid, M.M., Jacobs, C.R., *A finite element model of the human knee joint for the study of tibio-femoral contact.* Journal of Biomechanical Engineering, 2002. **124**(3): p. 273-80.

87. Knecht, S., et al., *MRI-based inverse finite element approach for the mechanical assessment of patellar articular cartilage from static compression test.* Biomed Tech (Berl), 2008. **53**(6): p. 285-91.

88. Mackerle, J., *Finite element modeling and simulations in orthopedics: a bibliography 1998-2005.* Comput Methods Biomech Biomed Engin, 2006. **9**(3): p. 149-99.

89. Elias, J.J. and A.J. Cosgarea, *Computational modeling: an alternative approach for investigating patellofemoral mechanics.* Sports Med Arthrosc, 2007. **15**(2): p. 89-94.

90. Weiss, J.A., et al., *Three-dimensional finite element modeling of ligaments: technical aspects.* Med Eng Phys, 2005. **27**(10): p. 845-61.

91. Anderson, A.E., Ellis, B.J., Maas, S.A., *Validation of finite element predictions of cartilage contact pressure in the human hip joint.* Journal of Biomechanical Engineering, 2008. **130**(5): p. 051008.

92. Ulrich, D., van Rietbergen, B., Laib, A., Ruegsegger, P., *Load transfer analysis of the distal radius from in-vivo high-resolution CT-imaging.* J Biomech, 1999. **32**(8): p. 821-8.

93. Ledoux, P., Lamblin, D., Targowski, R., *Modifications to the mechanical behavior of the wrist after fracture of the scaphoid. Modeling by finite element analysis.* Acta Orthop Belg, 2001. **67**(3): p. 236-41.

94. Carrigan, S.D., Whiteside, R.A., Pichora, D.R., Small, C.F., *Development of a three-dimensional finite element model for carpal load transmission in a static neutral posture.* Ann Biomed Eng, 2003. **31**(6): p. 718-25.

95. Liu, J., et al., *Rigid model-based 3D segmentation of the bones of joints in MR and CT images for motion analysis.* Med Phys, 2008. **35**(8): p. 3637-49.

96. Garcia-Elias, M., An, K.N., Cooney, W.P., Linscheid, R.L., Chao, E.Y., *Transverse stability of the carpus. An analytical study.* J Orthop Res, 1989. **7**(5): p. 738-43.

97. Horii, E., Garcia-Elias, M., Bishop, A.T., Cooney, W.P., Linscheid, R.L., Chao, E.Y., *Effect on force transmission across the carpus in procedures used to treat Kienbock's disease.* J Hand Surg [Am], 1990. **15**(3): p. 393-400.

98. Kwak, S.D., Blankevoort, L., Ateshian, G.A., *A Mathematical Formulation for 3D Quasi-Static Multibody Models of Diarthrodial Joints.* Comput Methods Biomech Biomed Engin, 2000. **3**(1): p. 41-64.

99. Pillai, R.R., et al., *MRI-based modeling for evaluation of in vivo contact mechanics in the human wrist during active light grasp.* Journal of Biomechanics, 2007. **40**(12): p. 2781-2787.

100. Pillai, R.R., Thoomukuntla, B.R., Ateshian, G.A., Fischer, K.J., *MRI-based modeling for evaluation of in vivo contact mechanics in the human wrist during active light grasp.* J Biomech, 2007. **40**(12): p. 2781-7.

101. Thoomukuntla, B., et al., *Preliminary Validation of MRI-Based Modeling For Evaluation of Joint Mechanics.* Journal of Musculoskeletal Research, 2008. **11**(4): p. 161-171.

102. Thoomukuntla, B.R., McIff, T.E., Ateshian, G.A., Bilgen, M., Toby, E.B., *Fischer, K.J.*, *Preliminary validation of MRI-based modeling for evaluation of joint mechanics.* Journal of Musculoskeletal Research (*in press*).

103. Waller, A.J., *Refinement and validation of MRI-based models for joint contact mechanics,* in *Mechanical Engineering*. 2007, University of Kansas: Lawrence.

104. Johnson, J.E., *Validation Of Radiocarpal Contact Models Based On Images From A Clinical MRI Scanner,* in *Mechanical Engineering*. 2008, University of Kansas: Lawrence.

105. Ray, R.D., R.J. Johnson, and R.M. Jameson, *Rotation of the forearm; an experimental study of pronation and supination.* J Bone Joint Surg Am, 1951. **33-A**(4): p. 993-6.

106. N.Soucacos, P. and N. A.Darlis, *The Distal Radio-Ulnar Joint: Functional Anatomy, Biomechanics, Instability and Management.* European Instructional Lectures, 2009. **Volume 9**: p. 115-124.

107. Milch, H., *So-Called Dislocation of the Lower End of the Ulna.* Ann Surg, 1942. **116**(2): p. 282-92.

108. Matsuki, K.O., et al., *In vivo 3D kinematics of normal forearms: analysis of dynamic forearm rotation.* Clinical biomechanics, 2010. **25**(10): p. 979-83.

109. Gardner, M.J., J.J. Crisco, and S.W. Wolfe, *Carpal kinematics.* Hand Clin, 2006. **22**(4): p. 413-20; abstract v.

110. Patterson, R.M., et al., *Carpal kinematics during simulated active and passive motion of the wrist.* J Hand Surg Am, 2007. **32**(7): p. 1013-9.

111. Sarrafian, S.K., J.L. Melamed, and G.M. Goshgarian, *Study of wrist motion in flexion and extension.* Clin Orthop Relat Res, 1977(126): p. 153-9.

112. Snel, J.G., et al., *Quantitative in vivo analysis of the kinematics of carpal bones from three-dimensional CT images using a deformable surface model and a three-dimensional matching technique.* Med Phys, 2000. **27**(9): p. 2037-47.

113. Marai, G.E., et al., *Estimating joint contact areas and ligament lengths from bone kinematics and surfaces.* IEEE Trans Biomed Eng, 2004. **51**(5): p. 790-9.

114. Cole, D.W., et al., *Distal radioulnar joint instability in distal radius fractures: the role of sigmoid notch and triangular fibrocartilage complex revisited.* Injury, 2006. **37**(3): p. 252-8.

115. Olerud, C., J. Kongsholm, and K.A. Thuomas, *The congruence of the distal radioulnar joint. A magnetic resonance imaging study.* Acta Orthop Scand, 1988. **59**(2): p. 183-5.

116. Poitevin, L.A., *Anatomy and biomechanics of the interosseous membrane: its importance in the longitudinal stability of the forearm.* Hand Clin, 2001. **17**(1): p. 97-110, vii.

117. Lichtman, D.M. and A. Joshi, *Acute injuries of the distal radioulnar joint and triangular fibrocartilage complex.* Instr Course Lect, 2003. **52**: p. 175-83.

118. Adams, B.D., *Distal radioulnar joint instability.* Instr Course Lect, 1998. **47**: p. 209-13.

119. Alexander, A.H. and D.M. Lichtman, *Kienbock's disease.* Orthop Clin North Am, 1986. **17**(3): p. 461-72.

120. Cheng, H.S., et al., *An analysis of causes and treatment outcome of chronic wrist pain after distal radial fractures.* Hand Surg, 2008. **13**(1): p. 1-10.

121. Bradway, J.K., P.C. Amadio, and W.P. Cooney, *Open reduction and internal fixation of displaced, comminuted intra-articular fractures of the distal end of the radius.* J Bone Joint Surg Am, 1989. **71**(6): p. 839-47.

122. Trumble, T.E., S.R. Schmitt, and N.B. Vedder, *Factors affecting functional outcome of displaced intra-articular distal radius fractures.* J Hand Surg Am, 1994. **19**(2): p. 325-40.

123. Voorhees, D.R., et al., *Carpal ligamentous disruptions and negative ulnar variance.* Skeletal Radiol, 1985. **13**(4): p. 257-62.

124. Watson, H.K. and F.L. Ballet, *The SLAC wrist: scapholunate advanced collapse pattern of degenerative arthritis.* J Hand Surg Am, 1984. **9**(3): p. 358-65.

125. De Smet, L., *Ulnar variance: facts and fiction review article.* Acta Orthop Belg, 1994. **60**(1): p. 1-9.

126. Trumble, T., et al., *A biomechanical comparison of the methods for treating Kienbock's disease.* J Hand Surg Am, 1986. **11**(1): p. 88-93.

127. Shaaban, H., et al., *The load-bearing characteristics of the forearm: pattern of axial and bending force transmitted through ulna and radius.* J Hand Surg Br, 2006. **31**(3): p. 274-9.

128. Viegas, S.F., et al., *The effects of various load paths and different loads on the load transfer characteristics of the wrist.* J Hand Surg Am, 1989. **14**(3): p. 458-65.

129. Viegas, S.F. and R.M. Patterson, *Load mechanics of the wrist.* Hand Clin, 1997. **13**(1): p. 109-28.

130. Viegas, S.F., et al., *Ulnar-sided perilunate instability: an anatomic and biomechanic study.* J Hand Surg Am, 1990. **15**(2): p. 268-78.

131. Viegas, S.F., et al., *Load transfer characteristics of the wrist. Part II. Perilunate instability.* J Hand Surg Am, 1987. **12**(6): p. 978-85.

132. Viegas, S.F., et al., *Load transfer characteristics of the wrist. Part I. The normal joint.* J Hand Surg Am, 1987. **12**(6): p. 971-8.

133. Tencer, A.F., et al., *Pressure distribution in the wrist joint.* J Orthop Res, 1988. **6**(4): p. 509-17.

134. Hlavacek, M. and D. Vokoun, *The influence of articular surface incongruity on lubrication and contact pressure distribution of loaded synovial joints.* Proc Inst Mech Eng H, 1998. **212**(1): p. 11-22.

135. Mino, D.E., A.K. Palmer, and E.M. Levinsohn, *Radiography and computerized tomography in the diagnosis of incongruity of the distal radio-ulnar joint. A prospective study.* J Bone Joint Surg Am, 1985. **67**(2): p. 247-52.

136. Zlatkin, M.B. and T. Greenan, *Magnetic resonance imaging of the wrist.* Magn Reson Q, 1992. **8**(2): p. 65-96.

137. Skahen, J.R., 3rd, et al., *Magnetic resonance imaging of the triangular fibrocartilage complex.* J Hand Surg Am, 1990. **15**(4): p. 552-7.

138. Hara, T., et al., *Force distribution across wrist joint: application of pressure-sensitive conductive rubber.* J Hand Surg Am, 1992. **17**(2): p. 339-47.

139. Nishiwaki, M., et al., *Ulnar-shortening effect on distal radioulnar joint pressure: a biomechanical study.* J Hand Surg Am, 2008. **33**(2): p. 198-205.

140. af Ekenstam, F., et al., *Corrective osteotomy of malunited fractures of the distal end of the radius.* Scand J Plast Reconstr Surg, 1985. **19**(2): p. 175-87.

141. Shaaban, H., et al., *Contact area inside the distal radioulnar joint: effect of axial loading and position of the forearm.* Clin Biomech (Bristol, Avon), 2007. **22**(3): p. 313-8.